https://doi.org/10.5194/acp-2022-505
Preprint. Discussion started: 22 July 2022

Atmospheric Chemistry and Physics Discussions

Vertical structure of the lower-stratospheric moist bias in the ERA5 reanalysis and its connection to mixing processes

Konstantin Krüger[1], Andreas Schäfler[1], Martin Wirth[1], Martin Weissmann[3], and George C. Craig[2]

[1]Deutsches Zentrum für Luft- und Raumfahrt (DLR), Institut für Physik der Atmosphäre, Oberpfaffenhofen, Germany
[2]Meteorologisches Institut München, Ludwig-Maximilians-Universität, Munich, Germany
[3]Institut für Meteorologie und Geophysik, Universität Wien, Vienna, Austria

Correspondence to: Konstantin Krueger (konstantin.krueger@dlr.de)

Abstract

Numerical weather prediction models (NWP) are known to possess a distinct moist bias in the mid-latitude lower stratosphere which is expected to affect the ability to accurately predict weather and climate. This paper investigates the vertical structure of this bias in the European Centre for Medium-Range Weather Forecast's (ECMWF) latest global reanalysis ERA5 using a unique multi-campaign data set of highly-resolved water vapor profiles observed with a differential absorption lidar (DIAL) onboard the High Altitude and LOng Range Research Aircraft (HALO). In total, 41 flights in the midlatitudes provide more than 31000 humidity profiles varying by four orders of magnitude. The data set covers different synoptic situations and seasons and thus is suitable to characterize the strong vertical gradients in the upper troposphere and lower stratosphere (UTLS). The comparison to ERA5 indicates high positive and negative deviations in the UT which on average lead to a slightly positive bias (+20 %). In the LS, the bias rapidly increases up to a maximum of +55 % at 1.3 km altitude above the thermal tropopause (tTP), and decreases again to 15-20 % at 4 km altitude. This vertical structure is reproduced in all flights. The depth of the layer of increased bias is smaller at high tropopause altitudes and larger when the tropopause is located low. Our results also suggest a seasonality of the bias, with the maximum in summer exceeding fall by up to a factor of 3. During one field campaign, co-located ozone and water vapor profile observations enable a classification of the observations into tropospheric, stratospheric and mixed air using H_2O-O_3 correlations. It is shown that the bias is higher in the mixed air while being small in tropospheric and stratospheric air which highlights that excessive transport of moisture into the LS plays a decisive role for the formation of the bias. Future climatological studies should consider the analysed lower-stratospheric moist bias in ERA5. Our results show that a better representation of mixing processes in NWP models could lead to a reduced LS moist bias that, in turn, may have a positive impact on weather and climate forecasts. The moist bias should be borne in mind for climatological studies using reanalysis data.

https://doi.org/10.5194/acp-2022-505
Preprint. Discussion started: 22 July 2022

Atmospheric Chemistry and Physics Discussions

1 Introduction

Water vapor is one of the most important greenhouse gases in the atmosphere and plays a key role for accurately predicting the Earth's weather (Gray et al., 2014; Shepherd et al., 2018) and climate (Forster and Shine, 2002; Riese et al., 2012). Through emission and absorption of radiation, water vapor impacts the temperature profile and thus is the main driver of the natural greenhouse effect (e.g., Held and Soden, 2000). In the upper troposphere and lower stratosphere (UTLS), defined as a layer located ± 5 km around the thermal tropopause (tTP) (Gettelman et al., 2011), rapidly decreasing water vapor concentrations in the vertical (e.g., Kiemle et al., 2012; Kaufmann et al., 2018) are of key relevance to a net cooling near and above the tropopause (Randel et al., 2007). The modulation of the vertical temperature gradients may influence the near tropopause potential vorticity (PV) gradients (Chagnon et al., 2013) that act as a waveguide for Rossby-waves (Martius et al., 2010) and thus may affect downstream weather development in the midlatitudes (e.g., Grams et al., 2011). Hence, an accurate representation of UTLS water vapor in numerical weather prediction (NWP) and climate models is essential.

In the extratropical UTLS, the distribution of water vapor is driven by transport processes related to baroclinic waves and associated synoptic and meso-scale weather systems (e.g., Gettelman et al., 2011; Schäfler et al., 2022, in prep.). Above the tropopause, increased static stability (Birner et al., 2002) impedes water vapor from being vertically transported. Correspondingly, the sharpest decline of water vapor is found just above the tropopause. Exchange processes affect the water concentration around the tropopause (Holton et al., 1995; Stohl et al., 2003) and create the extratropical transition layer (ExTL; Pan et al., 2004; Hoor et al., 2010) with influences of the troposphere and the stratosphere. In particular quasi-isentropic exchange near the polar and subtropical jets (Haynes and Shuckburgh, 2000) and cross-isentropic mixing, for instance through overshooting convection (Dessler and Sherwood, 2004; Homeyer et al., 2014), are major contributors to increased humidity above the tropopause. Furthermore, tropopause folds are known to be related to mass exchange between the UT and the LS (Shapiro et al., 1980). Above the ExTL, the concentration of water vapor approaches a low and vertically constant background value (e.g., Hintsa et al., 1994) which is determined by the stratospheric transport from tropics (Fueglistaler et al., 2009) within the Brewer-Dobson-Circulation (e.g., Dobson et al., 1946; Brewer, 1949) on time scales from months to years. The complexity of transport and mixing processes is mirrored in the high variability of water vapor in the extratropical UTLS on synoptic and seasonal time scales (e.g., Pan et al., 2000; Randel and Wu, 2010; Zahn et al., 2014; Dyroff et al., 2015; Bland et al., 2021; Schäfler et al., 2022, in prep.).

The sharp vertical gradients of trace species, PV, wind, and temperature at the extratropical tropopause are challenging to resolve for state-of-the-art NWP models (e.g., Stenke et al., 2008; Schäfler et al., 2020). Current operational analyses and forecasts are known to possess a distinct moist bias in the extratropical LS which is causing a co-located cold bias (Stenke et al., 2008; Diamantakis and Flemming, 2014; Shepherd et al., 2018). Recently, Bland et al. (2021) used radiosonde observations of a two-month period in fall and confirmed the earlier documented moist bias (about 70 % in the LS) in current operational analyses and forecasts of the European Centre for Medium-Range Weather Forecast's (ECMWF) Integrated Forecast System (IFS) and the Met Office's Unified Model (METUM) and a co-located cold bias. For a comprehensive overview of the studies

https://doi.org/10.5194/acp-2022-505
Preprint. Discussion started: 22 July 2022


Atmospheric Chemistry and Physics Discussions

that quantified the LS moist bias in different NWP systems, the interested reader is referred to Table 1 in Bland et al. (2021). The vertical structure of the bias was characterized by a small positive bias below the thermal tropopause followed by a vertical increase in the LS to a maximum at 1-2 km above the tropopause (e.g., Dyroff et al., 2015; Bland et al., 2021). However, contradictory results were obtained for the shape of the bias above its maximum. Bland et al. (2021) show an opposing vertical structure beyond 2 km above the tTP for two different radiosonde types. Woiwode et al. (2020) find cases with vertically decreasing and others with constant bias in IFS analysis and forecast data which are compared with humidity cross sections of an airborne passive infrared imager.

The origin of the wet model bias is still under debate: One hypothesis is, that the bias is caused by misrepresented dynamical transport and mixing processes, e.g. overshooting-convection leading to excessive water vapor injection into the LS (Kunz et al., 2014; Shepherd et al., 2018). Another potential source of overestimated transport of moisture into the LS is numerical diffusion and insufficient model resolution in the advection scheme of the semi-Lagrangian ECWMF models leading to an excessive diffusive transport of moisture across strong gradients from high to low mixing ratios (Stenke et al., 2008; Kunz et al., 2014; Dyroff et al., 2015; Shepherd et al., 2018). However, a LS moist bias of similar order is also found for widely-used "Eulerian" formulated models (Jiang et al., 2015; Davis et al., 2017). Moreover, the bias does not show a significant response to higher/lower horizonal, vertical or temporal model resolution (Woiwode et al. 2020), although this result may be affected by a moist bias that is already present in the initial conditions.

The above-mentioned studies used a variety of observation techniques to quantify the moist bias. Radiosonde or dropsonde humidity observations provide temporally continuous series of profiles at the same location, but their reliability is limited at highest altitudes (e.g., Bland et al., 2021). In-situ aircraft observations, even though very accurate and highly resolved, provide profile information only during start and landing and on flight routes of commercial or research aircraft (Zahn et al., 2014; Kunz et al., 2014; Dyroff et al., 2015; Kaufmann et al., 2018). On the contrary, space-borne microwave sounder provide humidity information across the entire globe but are limited in vertical resolution (e.g., Hegglin et al., 2009; Jiang et al., 2015). In between the in-situ and satellite observations, profile data from active and passive remote sensing instruments onboard research aircraft demonstrated the potential to characterize humidity across the tropopause (Ehret et al., 1999; Flentje et al., 2007; Woiwode et al., 2020; Schäfler et al., 2021), combining high spatial coverage, high accuracy and high vertical resolution (Bhawar et al., 2011). Since 2013, the active Differential Absorption Lidar (DIAL) WAter vapor and Lidar Experiment in Space (WALES; Wirth et al., 2009) has been deployed in several research campaigns onboard the High-Altitude and Long-Range aircraft (HALO; Krautstrunk and Giez, 2012) for water vapor profile measurements.

The goal of this paper is to evaluate the LS moist bias in the ECMWF's most recent global reanalysis ERA5. We suppose that potentially misrepresented mixing processes determine the vertical structure of the lower-stratospheric bias. To evaluate the model analyses, they are compared against a comprehensive data set of water vapor profiles observed by the airborne DIAL WALES in the mid-latitude UTLS. Co-located water vapor and ozone profiles are used to separate tropospheric, stratospheric and mixed air and individually assess the bias. The following three specific questions are addressed:

https://doi.org/10.5194/acp-2022-505
Preprint. Discussion started: 22 July 2022


Atmospheric Chemistry and Physics Discussions

1. Does the multi-campaign DIAL data set provide information for a robust quantification of the LS moisture bias?
2. What is the vertical structure of the LS moist bias in ERA5, particularly at high altitudes?
3. Is the moist bias correlated to the distribution of mixed air masses in the UTLS?

This paper is outlined as follows: Section 2 provides an overview of the water vapor DIAL observations (Sect. 2.1), the ERA5 reanalysis (Sect. 2.2) and the methods utilized to compare the observational and model data (Sect. 2.3). In Sect. 3.1 an example cross section of specific humidity and the bias are illustrated for a mid-latitude jet stream crossing which is followed by a statistical tropopause relative evaluation of the vertical structure of the bias and its variability in Sect. 3.2. The relationship between the bias and air mass classes in the UTLS is investigated in Sect. 3.3. Thereafter, Sect. 4 provides a discussion of the results. The key conclusions are summarized in Sect. 5.

2 Data and Methods

2.1 The WALES data set

The DIAL WALES (Wirth et al., 2009) was developed at the German Aerospace Center (DLR) and has been operated onboard the German research aircraft HALO since 2010. The instrument design is based on two identical laser systems that generate four wavelengths in the near-infrared (NIR) absorption band of H_2O between 935 and 936 nm allowing water vapor observations from the planetary boundary layer up to the stratosphere. WALES furthermore operates two polarization-sensitive channels at 1064 nm and at 532 nm. The latter channel comprises of a high-spectral resolution lidar (HSRL; Esselborn et al., 2008) enabling extinction coefficient observations and thus aerosol characterization (Groß et al., 2013). WALES and its underlying DIAL technique is briefly introduced in the following sequence and a more detailed description can be found in Wirth et al. (2009).

The four NIR wavelengths consist of three online channels (strongly absorbed by water vapor) and one offline channel (weakly absorbed). The number concentration of water vapor in the probed volume is derived from the ratio of the backscattered light of the on- and offline wavelengths and then converted to specific humidity. The online channels are sensitive to different trace gas concentrations, respectively different altitude levels. The exact wavelengths have been optimized such that they are optimally aligned to the moist boundary layer, the UT and the dry LS. Note, that WALES is able to measure humidity profiles in nearly cloud-free regions only. As extinction by cloud particles is too strong, no water vapor information can be retrieved within or below optically thick clouds.

Due to the photon statistics of the backscattered light as well as detector and background light noise, the retrieved water vapor profiles undergo statistical variations which are effectively reduced by temporal (i.e. horizontal) and vertical averaging. Thus, the retrieved DIAL water vapor profiles are averaged over 12 s or approximately 3 km in the horizontal. In the vertical, data is available every 15 m, although the effective vertical resolution is 300 m according to the full width of half maximum of the averaging kernel. It should be stressed, that the averaging kernel of a DIAL is exactly zero outside of about $\sqrt{2}$ times the

https://doi.org/10.5194/acp-2022-505
Preprint. Discussion started: 22 July 2022


Atmospheric Chemistry and Physics Discussions

effective resolution, depending on the numerical differentiation scheme. This is in sharp contrast to most passive remote sensing techniques and ensures that there is no uncontrolled leakage from moist to dry layer, which is of high importance for the analyses carried out within this work. Furthermore, systematic error sources such as Rayleigh-Doppler broadening of the beam or laser spectral impurity can also impact the precision, but are compensated for in the retrieval algorithm. A detailed error assessment of WALES and an intercomparison with other hygrometers (Kiemle et al., 2008) and with DIAL instruments (Bhawar et al., 2011) have proven the high measurement accuracy of WALES for various field campaigns. A comparison with a radiosonde equipped with a cryogenic frost-point hygrometer also provides a reference of the low uncertainty of WALES at low humidity values (Trickl et al., 2016). The data retrieval provides a parameter for the statistical error in the observed volume indicating the level of noise. The occurrence of "noisy" data is different for each flight and depends on the observed water vapor distribution and the background light situation. For instance, high noise levels are observed for dry air lying underneath moist air e.g. in the vicinity of stratospheric intrusions (Trickl et al., 2016). Filtering 5 % of the noisiest data for each individual flight turned out to be a useful threshold which predominantly reduced data availability in the lower-to-mid troposphere.

During one campaign WALES was operated in a different set-up to measure both water vapor and ozone, concurrently. For this purpose, two of the 935 nm NIR water vapor channels were replaced by two ultraviolet (UV) channels covering the 300-305 nm ozone absorption line (Fix et al., 2019). The use of two instead of four channels per trace gas leads to a reduced vertical coverage which was optimized so that the selected NIR wavelengths cover the tropopause region. Increased statistical noise required averaging in the retrieval over a period of 24 s (~6 km horizontally) while the effective vertical resolution remains approximately 300 m (Fix et al., 2019). Over the past decade, WALES was installed nadir-viewing onboard HALO and contributed to multiple research missions. Water vapor profiles were sampled along the flight track from the surface up to about 14 km altitude corresponding to the maximum flight level of the instrumented HALO (Krautstrunk and Giez, 2012). As the focus of this study is the mid-latitude UTLS, we only consider flights if they provide a significant amount of data across the tropopause. This was not the case for some campaigns that focused on the tropics where the tropopause level typically exceeded the flight level.

In total, DIAL data from six aircraft campaigns starting in 2013 are applied that provide more than 31000 water vapor profiles obtained during 41 flights (see Table 1). The majority (25) of the mission flights took place in the northern hemispheric fall season during the North Atlantic Waveguide Downstream impact EXperiment (NAWDEX; Schäfler et al., 2018) and the Wave-driven Isentropic Exchange campaign (WISE; Kunkel et al., 2019). As part of the campaigns ElUcidating the RolE of Cloud-Circulation Coupling in ClimAte (EUREC^{4}A; Stevens et al., 2021), the Next-Generation Aircraft Remote Sensing for Validation studies (NARVAL; Klepp et al., 2014) and NARVAL2 (Stevens et al., 2019) measurements were taken during eight flights in winter season. In addition, the Cirrus in High-Latitudes (Cirrus-HL) mission provides observations in summer. Figure 1 depicts the parts of HALO flight tracks with DIAL observations of all research flights that are considered in this study. Most flights were carried out over the North Atlantic between 48 °N and 66 °N, the North Sea and central to western Europe. Beyond this, the subtropics (>35 °N) and the Arctic are covered by individual flights as well.

https://doi.org/10.5194/acp-2022-505
Preprint. Discussion started: 22 July 2022

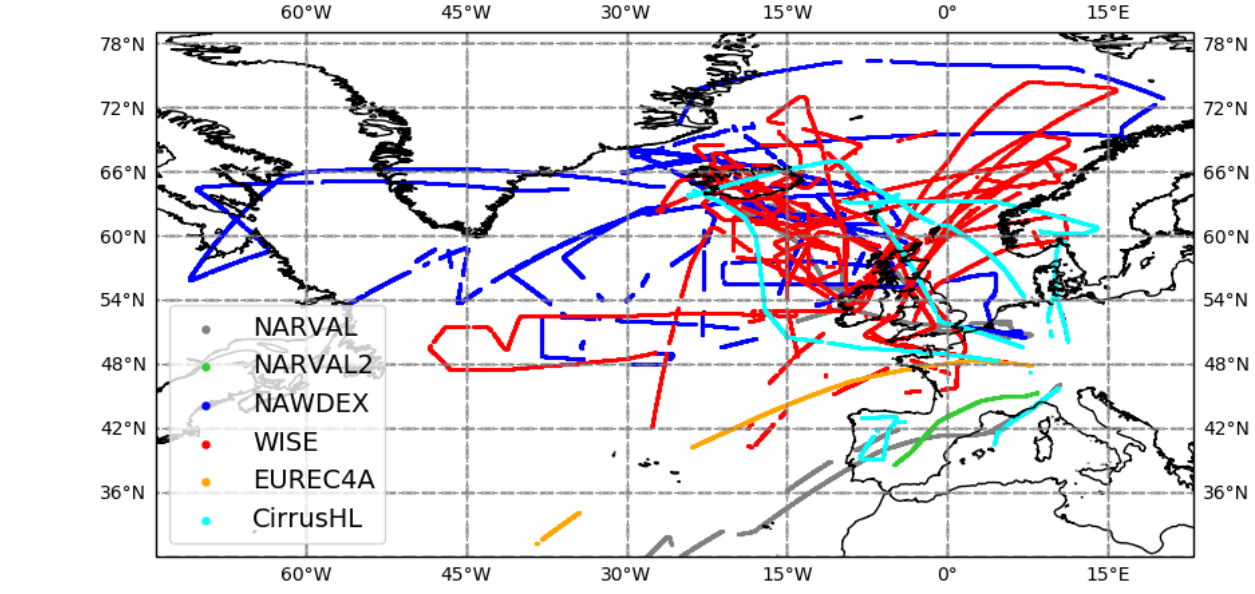

Figure 1: Map of HALO flight sections with WALES DIAL water vapor observations during the research campaigns NARVAL, NARVAL2, NAWDEX, WISE, EUREC^{4}A and Cirrus-HL (for detailed overview see Sect. 2.1).

The number of observations with respect to latitude (Fig. 2a) illustrates the high data availability in the midlatitudes, which is the region of major interest in this study. This data set that covers humidity observations in a broad spectrum of synoptic situations (e.g., extratropical cyclones or anticyclones) is considered to be representative for mid-latitude weather. Figure 2b shows the distribution of measured water vapor covering four orders of magnitude ranging from 10^{-3} to 10^{1} g kg^{-1}. The bimodal shape of the histogram is composed of a broad moist part that can be assigned to the troposphere and a fraction of low humidity representing the dry conditions in the stratosphere. Each campaign exhibits an individual footprint of measured humidity, depending on the season, observation areas and the flight level selection. For instance, the histograms for NAWDEX and WISE are remarkably similar since both campaigns took place over the North Atlantic in fall. However, as only two NIR wavelengths were operated to measure water vapor during WISE, less measurements are available at high humidity levels. NARVAL shows a distinctive dry spectrum of measured humidity corresponding to the winter season and less data is available for the LS, resulting from frequent low flight altitudes. The Cirrus-HL summer campaign stands out because a large proportion of high moisture values was observed. The NARVAL2 and the EUREC^{4}A campaign provide UTLS measurements only for one flight and thus, compared to the other field campaigns, provide a small number of observations (see also Table 1).

https://doi.org/10.5194/acp-2022-505
Preprint. Discussion started: 22 July 2022

Atmospheric Chemistry and Physics Discussions

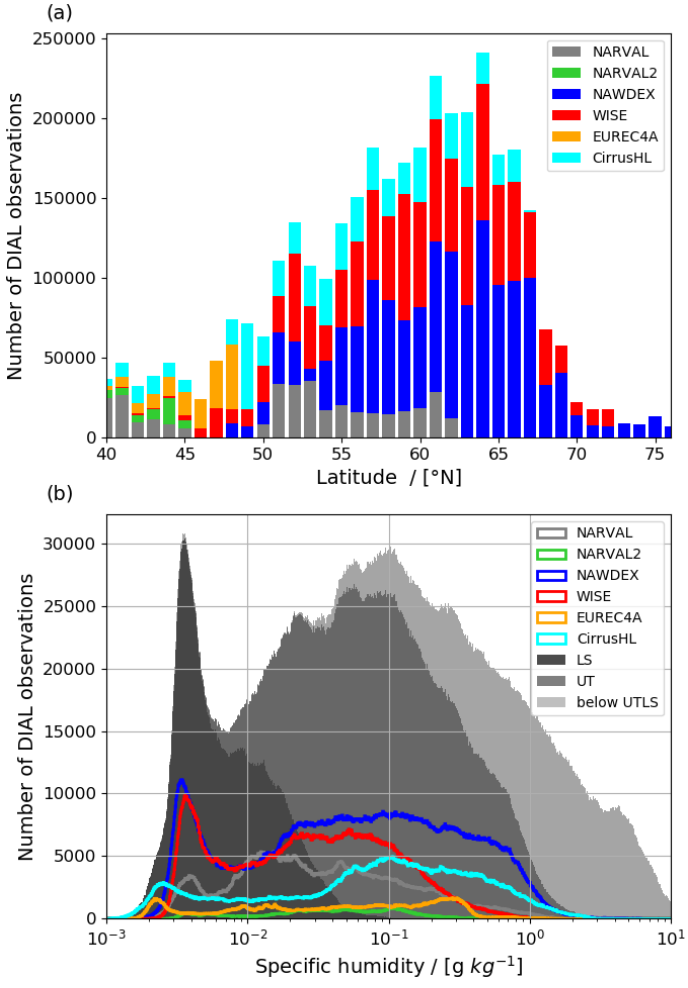

Figure 2: (a) Stacked distribution of the number observations per 1° bins of latitude and per individual campaigns (coloured bars). (b) Histogram of observations per humidity bin with size 0.01 g kg^{-1} of $\log_{10}(q_{DIAL})$ for individual campaigns in the UTLS (coloured lines) and separated for the LS (all data above the thermal tropopause, dark grey shading), the UT (all data between the tTP and 5 km below, medium grey shading) and the remaining tropospheric data (light grey shading).

https://doi.org/10.5194/acp-2022-505
Preprint. Discussion started: 22 July 2022

Table 1: Overview of all considered campaigns with DIAL observations. The number of DIAL profiles refers to all profiles that were sampled during the 41 flights. The number of DIAL profiles in the LS corresponds to all profiles with measurements in the LS and that are used in the statistical evaluation providing measurements above the thermal tropopause (see explanation in 2.3.1).

Campaign	Year Month	Season	Number of Flights (hours)	Flight distance (km)	Number of DIAL profiles	Number of DIAL profiles in LS
NARVAL	2013/14 Dec-Jan	Winter	7 (37)	31157	9937	4397
NARVAL2	2016 Aug	Summer	1 (9)	7729	2395	485
NAWDEX	2016 Sep-Oct	Autumn	11 (70)	55695	17745	11559
WISE	2017 Sep-Oct	Autumn	14 (98)	83041	12475	8709
EUREC^{4}A	2020 Jan-Feb	Winter	1 (8)	7011	2307	1583
Cirrus-HL	2021 Jun-Jul	Summer	7 (30)	23675	6777	4638
Total			41 (245)	208308	51636	31371

2.2 ERA5 reanalysis data

ERA5 is the latest generation reanalysis of the ECMWF based on the IFS Cycle 41r2 that was used for operational weather prediction at ECMWF in 2016. Atmospheric quantities are provided on a global grid with a horizontal resolution (TL639) of about 31 km, and on 137 hybrid sigma-pressure model levels ranging from the surface up to 0.01 hPa (~80 km) in the vertical. The altitude range with DIAL observations is covered by the lowermost 70 model levels. The vertical grid spacing of the model levels ranges from a few metres in the boundary layer to about 300 metres at the tropopause level (Schäfler et al., 2020). ERA5 reanalyses are available at one-hour intervals, which is an improvement compared to a six-hourly resolution of its predecessor ERA-Interim (Dee et al., 2011). Further details about ERA5 are documented in Hersbach et al. (2020). For this study, model level data is retrieved on a regular 0.36°x0.36° longitude/latitude grid. Pressure and altitude of each model level is derived following the IFS documentation (ECMWF, 2015). To be able to compare ERA5 and WALES data, the gridded model data is interpolated in space and time to the observation location. Our interpolation method uses on a horizontally bi-linear interpolation, followed by a linear interpolation in the vertical. Finally, a linear interpolation in time of the hourly ERA5 profiles towards the observation time is carried out. This sequence of interpolations has been applied similarly in other studies (e.g., Schäfler et al., 2010).

https://doi.org/10.5194/acp-2022-505
Preprint. Discussion started: 22 July 2022


Atmospheric Chemistry and Physics Discussions

2.3 Data Processing

2.3.1 Thermal tropopause detection

Due to the variable altitude of the tTP, the distribution of water vapor in the UTLS is also highly variable. Hence, horizonal averaging of the humidity profiles in geometrical coordinates strongly blurs the vertical gradients across the tropopause. Therefore, bias statistics are often performed in tropopause relative coordinates (e.g., Kunz et al., 2014; Bland et al., 2021). Different tropopause definitions have been established taking the thermal, dynamical and chemical properties of the UTLS as a reference. By definition, the tTP marks the reversal of the vertical temperature gradient and thus the abrupt increase in static stability which is reflected in the sharp distribution of trace species across the tropopause (Gettelman et al., 2011). We use the tTP as it best reflects the strongest vertical gradients of water vapor (Birner et al., 2002; Pan et al., 2004). For each profile, we calculate the tTP altitude following the lapse rate-based World Meteorological Organisation's (WMO) definition from the ERA5 temperature profile that is interpolated to the 15 m vertical grid of the lidar. A tropopause is detected as the lowest level at which the vertical temperature gradient Γ drops below +2 K km^{-1}. The tTP is only defined if the average lapse rate between this and any other level within a 2 km deep layer remains equal or lower than +2 K km^{-1} (WMO, 1957). The vertical temperature gradient, respectively the lapse rate, is computed following Eq. (1):

$$\Gamma = \left(-\frac{dT}{dz}\right)\left[\frac{K}{km}\right] \quad (1)$$

Recent studies have proven a high agreement between ECMWF IFS and radiosonde-derived tTP altitudes that lie within a few hundred metres except for complex tropopause fold situations (Bland et al., 2021). In our analyses, the tTP detection is started in upward direction from 5 km altitude in order to avoid misdetections of tropopauses due to local fluctuations of temperature in the lower-to-mid troposphere. When a tTP is detected, the (thermal) tropopause relative coordinates $z_{rel.tTP}$ are derived by simply subtracting the altitude of tTP (z_{tTP}) from the geometric height vector (z_{geom}) (see Eq. (2)).

$$z_{rel.tTP} = z_{geom} - z_{tTP} \quad (2)$$

There are atmospheric conditions in which tropopause detection is ambiguous, especially in the vicinity of jets and associated tropopause folds where double tropopauses can occur (e.g., Shapiro, 1980; Gettelman et al., 2011). We found that in situations of weak vertical temperature gradients near the jets, the lapse rate threshold in the WMO definition may lead to vertical jumps of the tTP altitudes for adjacent profiles. In tropopause relative coordinates these fluctuations result in wrongly allocated vertical distributions of water vapor. A detailed discussion will follow in Sect. 3.1.1. To remove such profiles in the overall statistic, we apply a filtering method based on mean potential vorticity (MPV; Shapiro et al. 1998) in which the average PV is calculated for the 5 km layer above and below the thermal tropopause. MPV thresholds of MPV < 3.5 PVU (1 PVU = 10^{-6} K m^2 kg^{-1} s^{-1}) above and > 3.5 PVU below the tTP are found to be an efficient metric to filter profiles within an erroneously assigned tTP. The vertical distribution of tTP altitudes of the 31371 profiles is shown in Fig. 3. The detected thermal tropopause altitudes lie between 5.5 km and more than 15 km altitude reflecting the broad spectrum of synoptic situations covered by the data set. The majority of all tTPs is found between 10 and 13 km which represents a typical location of the mid-latitude tropopause with respect to interannual or synoptic variations (e.g., Birner et al., 2002).

https://doi.org/10.5194/acp-2022-505
Preprint. Discussion started: 22 July 2022

Atmospheric Chemistry and Physics Discussions

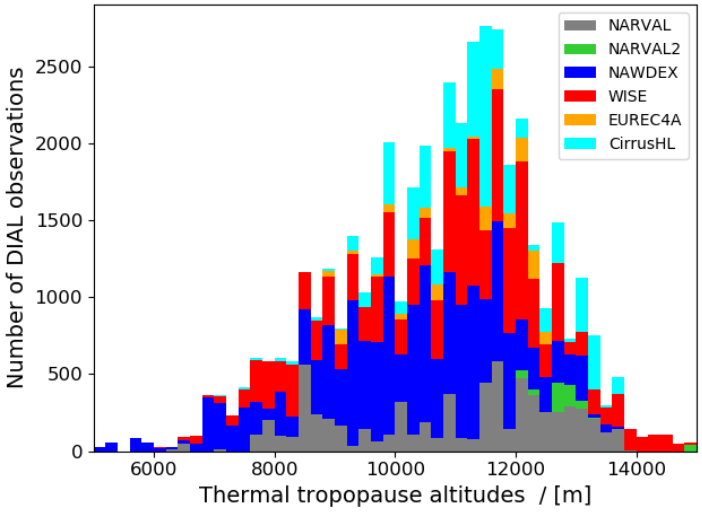

Figure 3: Histogram of the number of observations per thermal tropopause altitude bin (1000 m) and per campaign (coloured bars).

2.3.2 Statistical metric of the bias

The selection of a suitable statistical difference metric is crucial for a robust quantification of model humidity errors and different statistical approaches can be found in the literature (Kunz et al., 2014; Bland et al., 2021). As specific humidity rapidly decreases across the tropopause, absolute humidity differences are not appropriate and most studies rely on a relative formulation of the error. However, since the simple ratio of model and observation or the absolute bias divided by the observed value are statistical asymmetric quantities, we apply a logarithmic formulation (see Eq. (3)) introduced by Kunz et al. (2014):

$$humidity\ bias\ = log_2\left(\frac{Q_{ERA5}}{Q_{DIAL}}\right), \text{ with } Q_{DIAL} \text{ being the measured and } Q_{ERA} \text{ being the ERA5 specific humidity} \quad (3)$$

This unitless definition of the relative bias is symmetrically centred around zero and thus not distorted when averaged. A perfect agreement (relative bias = 0) between the ERA5 and the DIAL specific humidity is reached if $Q_{ERA5} = Q_{DIAL}$. A positive relative bias ϵ [0,∞] indicates an overestimation of humidity by the model ($Q_{ERA5} > Q_{DIAL}$), whereas a negative bias ϵ [-∞,0] implies an underestimation ($Q_{ERA5} < Q_{DIAL}$). Table 2 gives some values of the bias for example moisture observations.

https://doi.org/10.5194/acp-2022-505
Preprint. Discussion started: 22 July 2022

Atmospheric Chemistry and Physics Discussions

Table 2: Example values of specific humidity and the computed humidity bias.

Q_{ERA5}	g kg^{-1}	1,00	1,25	1,50	1,75	2,00	2,25	2,50	3,00
Q_{DIAL}	g kg^{-1}	1,00	1,00	1,00	1,00	1,00	1,00	1,00	1,00
Humidity bias	Unitless	0	0,32	0,58	0,81	1,00	1,17	1,32	1,58
Percentage	%	0	25	50	75	100	125	150	200

3 Results

3.1 Water vapor and bias distributions for a selected case

First, an example cross section of water vapor measurements of the research flight on 1st October 2017 during the WISE campaign is presented in Fig. 4. The case is selected as it possesses a good data coverage across the UTLS and as it additionally provides O_3 observations (see Sect. 3.3). HALO flew meridional transects over the North Atlantic (50°N-60°N) at 13°W aiming to measure a zonal jet stream and its associated predicted strong trace gas gradients. The underlying synoptic situation and the corresponding mission objectives are introduced in detail by Schäfler et al. (2021). The left part of Fig. 4a (up to a distance of roughly 800 km) illustrates the water vapor distribution north of the jet stream (see magenta isopleths) where the aircraft flew above the low-located tropopause within the LS. HALO then crossed the pronounced jet with wind velocities of more than 90 m s^{-1}. Near the core of the jet, the tTP altitude jumps from 6.5 to 14 km within a few kilometers flight distance. The dynamical tropopause (2 PVU contour line) also displays the ascent of the tropopause and a corresponding tropopause fold that extends along inclined isentropes into the mid-troposphere. In the right part of Fig. 4a, the air mass located to the south of the jet exhibits high tropopause altitudes exceeding the flight level by roughly 2 km, so that measurements are restricted to tropospheric air. Along the entire cross section, the highest specific humidity is observed at the lowest levels in the UT ranging from 10^{-2} g kg^{-1} to occasionally more than 10 g kg^{-1}. The tropospheric air to the south of the jet has an increased humidity content compared to the air northward from the jet. In the LS, specific humidity values smaller than 10^{-2} g kg^{-1} are frequently observed. At a first glance, the specific humidity curtain of ERA5 (Fig. 4b) is very similar to the observations. However, the ERA5 humidity field appears to be smoother, particularly in the presence of strong horizontal water vapor gradients, for instance, near the jet and mesoscale filaments. Relative differences between observations and model calculated by applying Eq. (3) are shown for the vertical section in Fig. 4c. Reddish regions indicate an overestimation of humidity by ERA5, while bluish areas represent underestimations. High positive and negative values of the bias alternate below the tropopause. In the LS, a coherent region of positive values is detected between 1 and 3 km above the tTP indicating an overestimated humidity which extends over the entire part north of the jet. At the highest altitudes, beyond 3 km above the tropopause, the bias is smaller. In order to study the systematic of the diagnosed LS bias and its vertical structure, a statistic of all data in tropopause relative coordinates is performed.

https://doi.org/10.5194/acp-2022-505
Preprint. Discussion started: 22 July 2022

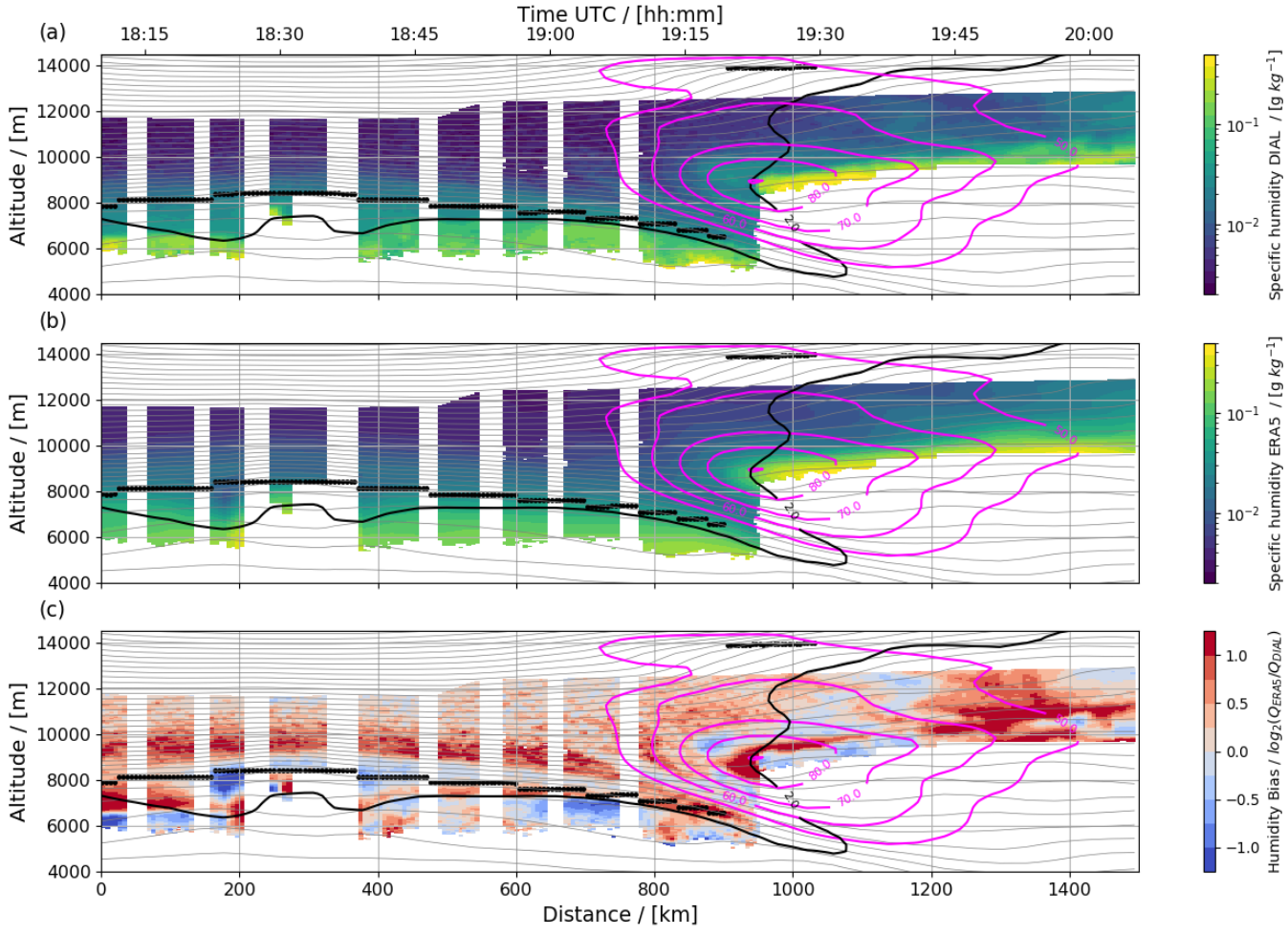

Figure 4: Vertical cross sections of (a) the DIAL specific humidity (colour shading, g kg^{-1}), (b) ERA5 specific humidity (colour shading, g kg^{-1}) as well as (c) the corresponding humidity bias (colour shading) on the 1st October 2017. Panels are superimposed by derived thermal (thick black dots) and dynamical tropopause (2 PVU, black isoline), potential temperature (grey contours, $\Delta\theta$ = 3K) and isopleths of the wind speed (magenta contours, in m s^{-1}).

3.2 Statistical analysis of the LS bias

3.2.1 Vertical structure

For all 41 flights, respectively 31371 profiles, the average profiles of specific humidity and the bias are presented in Fig. 5. The moisture profiles of WALES and ERA5 show an exponential decline of specific humidity in the UT, ranging from about 5x10^{-1} g kg^{-1} at the lowest levels to approx. 3x10^{-2} g kg^{-1} at the tropopause level. The strongest vertical gradient occurs in a layer of 0.5 to 1 km above the tropopause. Beyond, a less pronounced decline of water vapor extends until 4 km above the tropopause followed by a vertical constant specific humidity of about 3.5x10^{-3} g kg^{-1}. There is a high level of agreement

https://doi.org/10.5194/acp-2022-505
Preprint. Discussion started: 22 July 2022

Atmospheric Chemistry and Physics Discussions

between the ERA5 and WALES specific humidity profiles, particularly in the UT, although ERA5 appears to be moister at all altitudes. For both data sets, the median and arithmetic mean profiles of specific humidity slightly vary from each other. The median line is slightly shifted towards drier humidity values, most pronounced in the UT. Figure 5a also demonstrates a high
285 data availability throughout the entire UTLS. The number of observations is highest between -5 and +1 km around the tTP, with two local maxima at -2 km and roughly +1 km. Note, that these two peaks in data availability are related to the typical flight altitudes, either above or below the main transatlantic air traffic routes (Schäfler et al., 2018), and the maximum data coverage close to the aircraft. Above the tTP, the number of observations continuously decreases and roughly halves per kilometre altitude. At 4 km above the tTP ~3000 data points are available.

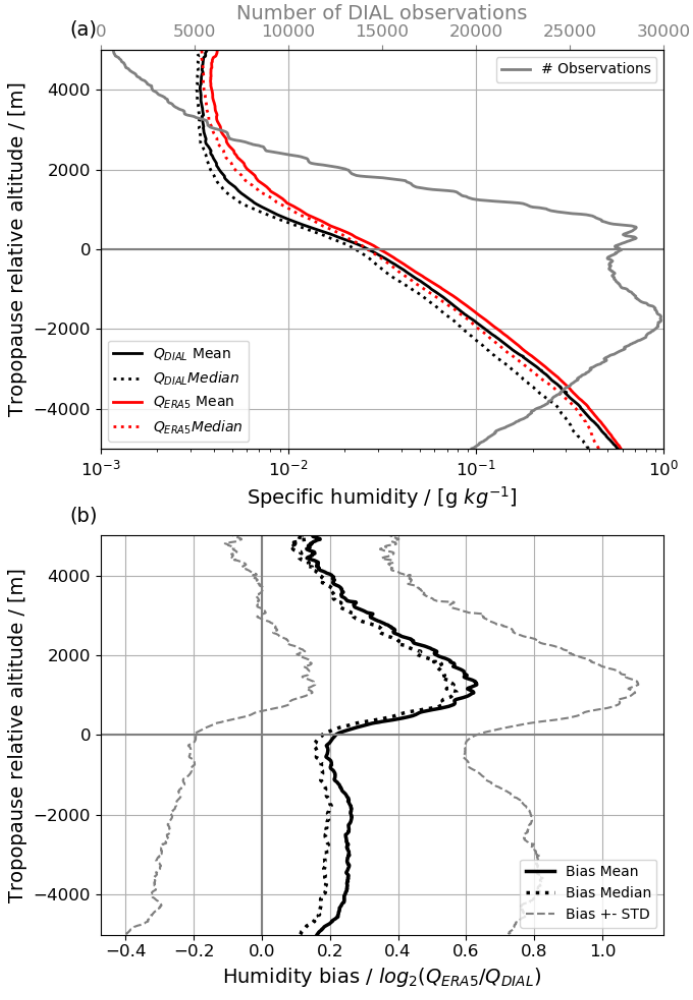

290

Figure 5: Tropopause-relative (a) vertical profiles of the DIAL (black lines) and the ERA5 (red lines) mean (solid) and median (dotted) specific humidity and the number of observations (grey). Note the log-scale notation of the x-axis. (b) Mean/median bias (solid/dotted lines) and standard deviation (grey dotted lines).

https://doi.org/10.5194/acp-2022-505
Preprint. Discussion started: 22 July 2022


Atmospheric Chemistry and Physics Discussions

The higher moisture values in the ERA5 data become apparent in the vertical profile of the bias (Fig. 5b) that is weakly positive (+0.2; 15 %) in the UT which is concomitant with a high standard deviation. This is a result of strong positive and negative bias values, as seen for example in the case study (Fig. 4c). The weakest bias is reached at the tTP level where the bias is smaller than 0.2 (<15 %). Above, the vertical moisture gradient at the tropopause level is stronger in observations leading to a significant overestimation of humidity in the LS up to 4 km above tTP. The bias increases to a maximum of +0.63 (55 %) at 1.3 km altitude above the tTP. Beyond, the bias reduces by roughly 0.2 per 500 m up to 4 km altitude above the tTP, where it is approx. +0.2 (15 %). At the highest altitudes a weak and vertically nearly constant bias is observed, although the sparse data coverage has to be noted. At the tropopause as well as above, the standard deviation is significantly reduced compared to the UT. Mean and median profiles of the relative bias slightly differ, but compared to the magnitude of the bias, these differences are very small. The maximum mean and median biases are +0.63 (55 %), respectively +0.58 (49 %).

To better illustrate the variability of the water vapor observations in the vertical, Fig. 6 shows the number of data and the mean bias in bins of tropopause relative altitude and specific humidity. Figure 6a indicates a broader observed distribution of water vapor in the UT compared to the LS. A small number of unusually low humidity values ($< 10^{-2}$ g kg^{-1}) is detected below the tropopause (-4 to -1 km) and on the other hand some data show high specific humidity ($> 10^{-2}$ g kg^{-1}) above the tTP (1-3 km). These data are related to profiles observed in complex tropopause situations with incorrectly assigned tropopause altitudes that were not removed by the applied MPV filtering (see Sect. 2.3.1). However, these remaining outliers are tolerable as they have a negligible impact on the statistics. Throughout the UT, a weak positive bias is detected in bins of highest data availability. At the edges of the distribution, highest humidity values show a negative bias while the lowest humidity values stand out due to positive bias (Fig. 6b). We found that this is related to a narrower distribution of ERA5 humidity compared the observations (not shown). However, the low number of observations at the edges should be noted here. In the LS the positive bias is higher and most pronounced up to 3.5 km above the tropopause and at very low specific humidity values. The positive bias reduces towards highest altitudes of the LS, although the reduced data coverage has to be kept in mind (Fig. 5a).

https://doi.org/10.5194/acp-2022-505
Preprint. Discussion started: 22 July 2022

Atmospheric Chemistry and Physics Discussions

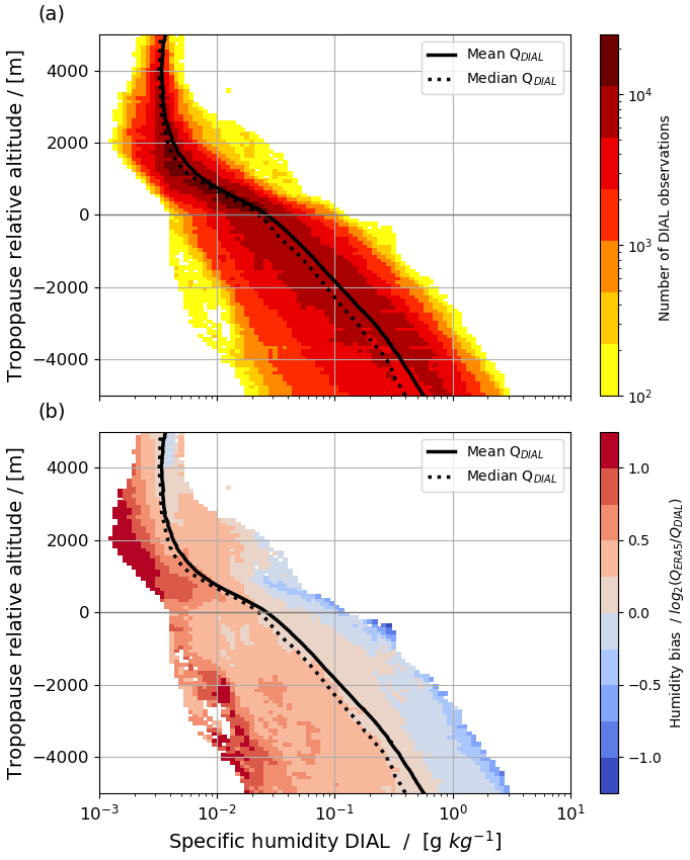

Figure 6: Binned distribution of DIAL specific humidity observations relative to the thermal tropopause coloured by (a) the number of observations per bin and (b) the bin-average humidity bias. Thick black solid (dotted) lines in (a) and (b) show mean (median) values per altitude bin. Bin sizes are 100 m and 0.01 g kg^{-1} of $\log_{10}(q_{DIAL})$. Please note the logarithmic abscissa and color bar in (a).

3.2.2 Synoptic and seasonal variability

In this section, the variability of the LS bias between flights, campaigns and tropopause altitudes is investigated. Figure 7 shows the observed humidity distribution within a 3 km layer above the tTP, i.e. the main area of the LS bias. For each flight, the observed median humidity values range from $1x10^{-2}$ to $4x10^{-3}$ g kg^{-1} and the interquartile range strongly vary between the individual flights, which presumably relates to differences in the flight level, the tropopause altitude, and the synoptic situation. During summer (Cirrus-HL) and fall campaigns (NAWDEX, WISE) the range of observed humidity is larger compared to the winter campaign (NARVAL). It is furthermore noticeable, that intra-campaign variations (=synoptic variability) of observed humidity exceed the seasonal variability. Per flight, the median LS bias (Fig. 7b) varies from 0.2 (15 %) to 1.4 (164 %) but a positive bias is detected for each flight. Whereas the magnitude of the bias shows no obvious correlation with the LS moisture distribution, the bias appears to be smaller in winter (NARVAL) compared to fall (NAWDEX, WISE). Interestingly, the bias

https://doi.org/10.5194/acp-2022-505
Preprint. Discussion started: 22 July 2022

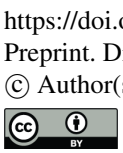

Atmospheric Chemistry and Physics Discussions

during the Cirrus-HL summer campaign is remarkably strong. The number of observations that is available for each flight is strongly variable between a few and several hundred thousand (Fig. 7c).

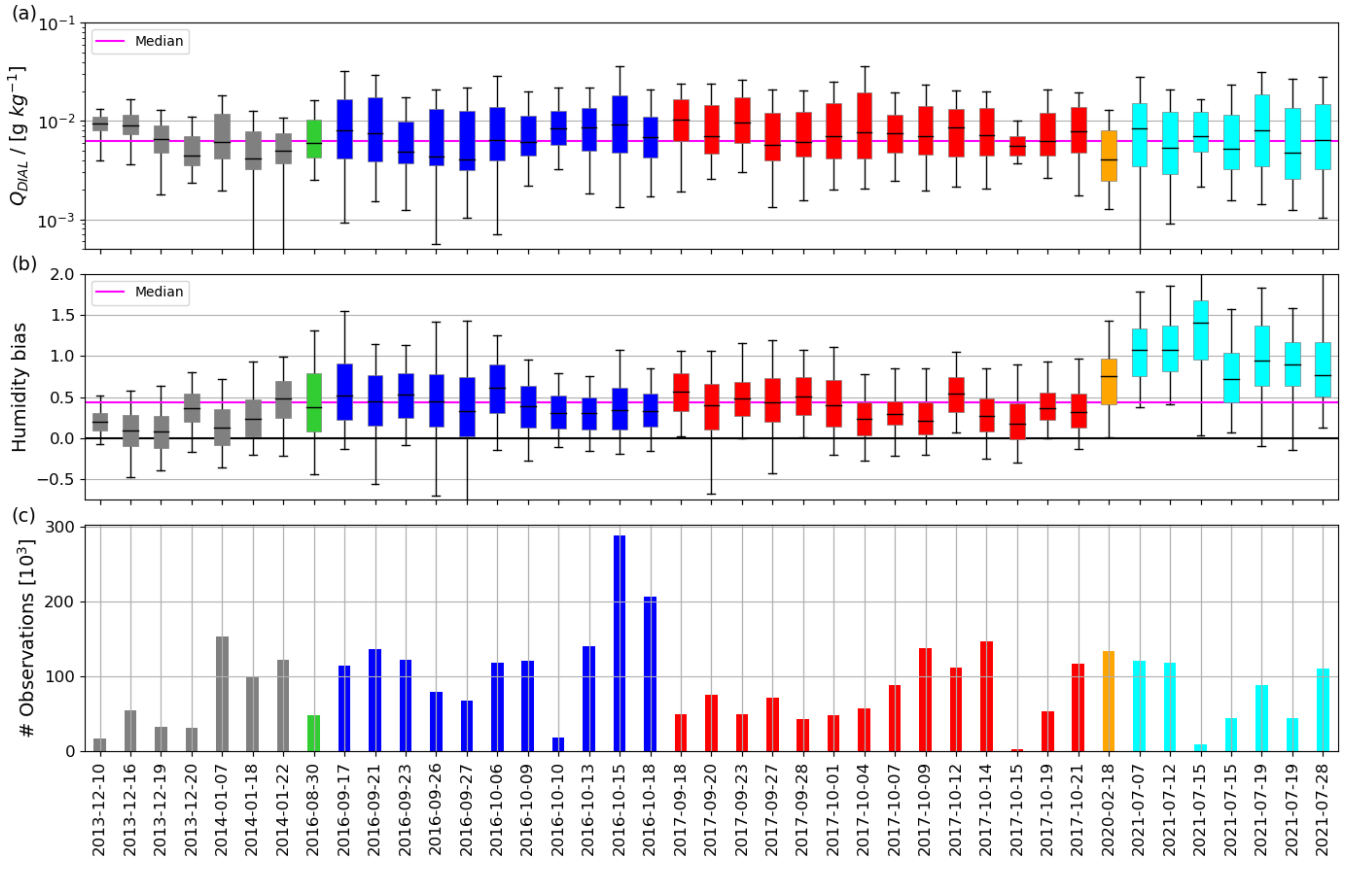

Figure 7: Distributions of (a) the observed humidity and (b) the humidity bias and (c) the number of data points for the layer 0 to +3 km above the thermal tropopause. The average observed humidity and bias for all flights is given by the magenta lines in (a) and (b). The boxes in (a) and (b) define the interquartile range located around the median (black) and the whiskers illustrate the 5th/95th percentile. The different campaigns are color-coded as in Fig. 1.

For each campaign, the average profile of the bias and the number of observations is shown in Fig. 8. The data availability, particularly at highest altitudes, is very different across the campaigns (Fig. 8b). During NAWDEX and WISE a large number of observations is present between -5 km below and +4 km above the tTP. Cirrus-HL provides approximately half as much data at each altitude except for altitudes beyond +3 km above the tTP where little data is available. The EUREC^{4}A and the NARVAL2 campaigns provide observations above the tropopause only during one flight so the small number of measurements limit the interpretation. Due to frequent low flight levels during the six NARVAL flights, only a small number of observations is available beyond +1 km above the tTP. The general structure including a pronounced positive bias, a local minimum at the tropopause, and a decrease towards the highest altitudes is maintained throughout the campaigns (Fig. 8a) although significant

https://doi.org/10.5194/acp-2022-505
Preprint. Discussion started: 22 July 2022

Atmospheric Chemistry and Physics Discussions

345 differences can be identified across the campaigns. For the fall campaigns in two successive years (NAWDEX and WISE) a similar shape of the bias is observed across the entire profile. The maximum bias is located at approximately the same altitude, and a similar decrease beyond this maximum is observed. However, the magnitude of the LS bias is slightly higher for NAWDEX (0.6, 50 %) compared to WISE (0.5, 40 %). During summer (Cirrus-HL), a strong bias is detected exceeding 1.20 (130 %) at its maximum. Compared to fall, the summer bias is increased by a factor of 2-3. During winter (NARVAL), the LS
350 bias is small (0.3, ~23 %) and not significantly higher than the upper-tropospheric bias, but the limited representativity due to the low number of observations should be noted here.

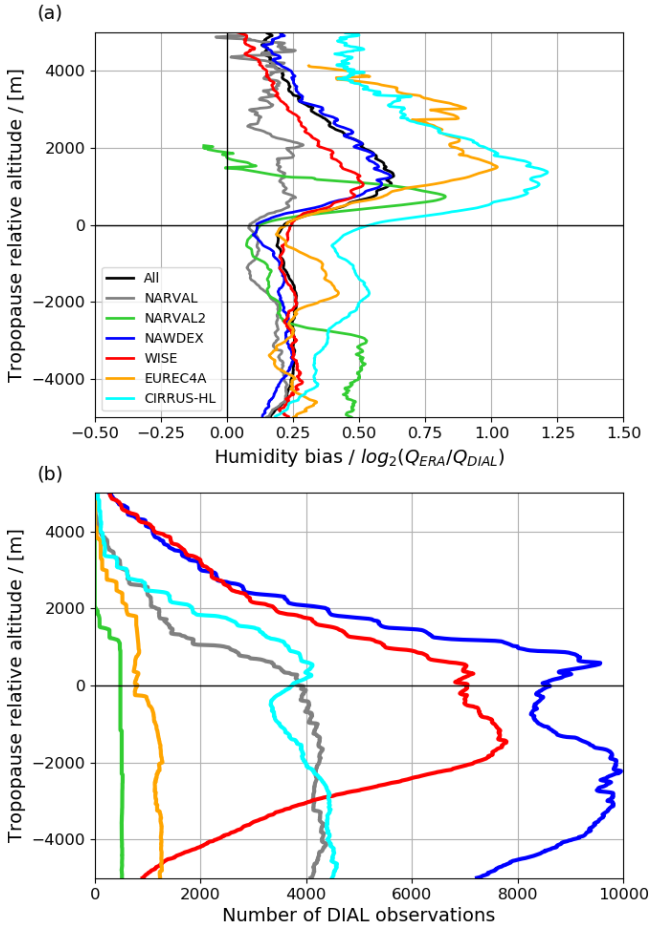

Figure 8: Tropopause-relative vertical profiles of (a) humidity bias and (b) number of observations for the different campaigns (colour coded as in Fig. 1). The black line represents the multi-campaign average.

355 In addition, we explore whether the observed vertical structure of the bias is sensitive to different synoptic situations. For this investigation, the DIAL profiles are classified by their corresponding tTP altitude. Lower tropopauses are typically associated with trough situations and high tropopauses occur above ridges. For each category the corresponding average bias profile and

https://doi.org/10.5194/acp-2022-505
Preprint. Discussion started: 22 July 2022

Atmospheric Chemistry and Physics Discussions

the number of observations is given in Fig. 9. The vertical structure of the bias apparent in Fig. 5b is reproduced for each tropopause altitude interval. No systematic differences between the bias profiles can be revealed in the UT. Interestingly, each category shows an increased bias of comparable magnitude as well as a decrease above, although its vertical position relative to the tTP is different. The maximum bias is located higher for low tropopause altitudes, while profiles with high tTP altitude show a maximum closer to the tTP. For instance, the maximum bias for low tropopauses (< 8 km) is located at +2 km above the tTP, while for the category with highest tropopauses (12-14 km) the maximum value is found at +1 km. The number of data points illustrates that each category exhibits a reasonable number of observations (Fig. 9b).

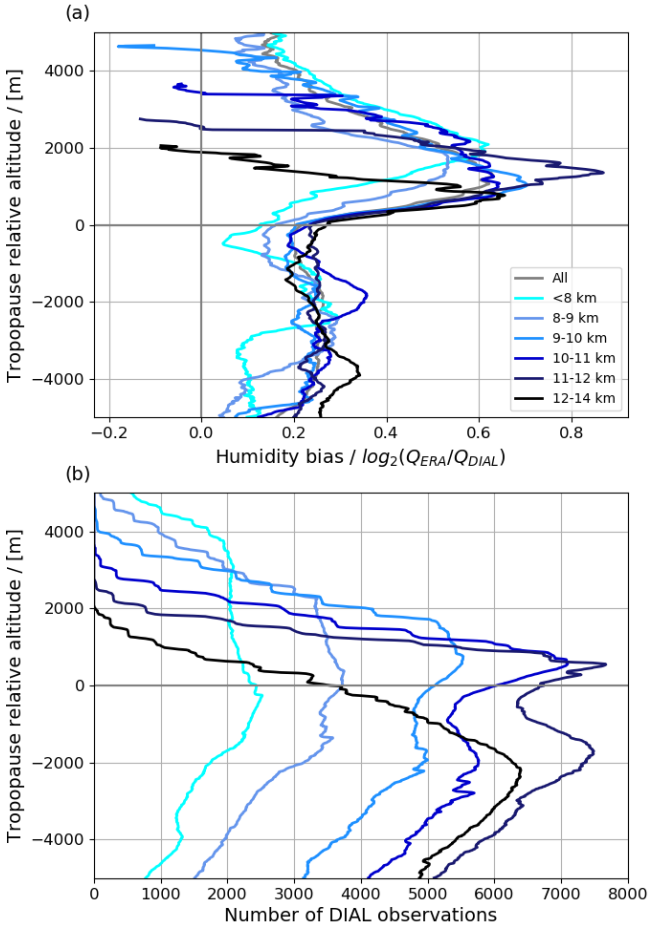

Figure 9: Tropopause-relative profiles of the (a) humidity bias and (b) number of observations for different intervals of tTP altitudes (colour coded).

3.3 The vertical structure of the bias related to mixing processes

In the following it is examined to what extent the observed air masses have experienced mixing in their history and whether this is related to the vertical structure of the bias. For this purpose, we examine co-located ozone and water vapor observations

https://doi.org/10.5194/acp-2022-505
Preprint. Discussion started: 22 July 2022

Atmospheric Chemistry and Physics Discussions

that were collected during four WISE research flights that provide a suitable data coverage. First, the observed ozone distribution for the same case study as introduced in section 3.1 is illustrated in Fig. 10a. The distribution of ozone is opposite to that of water vapor, with lowest concentrations (< 100 ppb VMR) in the troposphere and an increase with altitude across the tropopause to more than 500 ppb VMR. Note the filamentary structures of increased ozone values in the LS and the ozone-
375 rich air which is transported downward within the tropopause fold (see detailed description in Schäfler et al., 2022, in prep.).

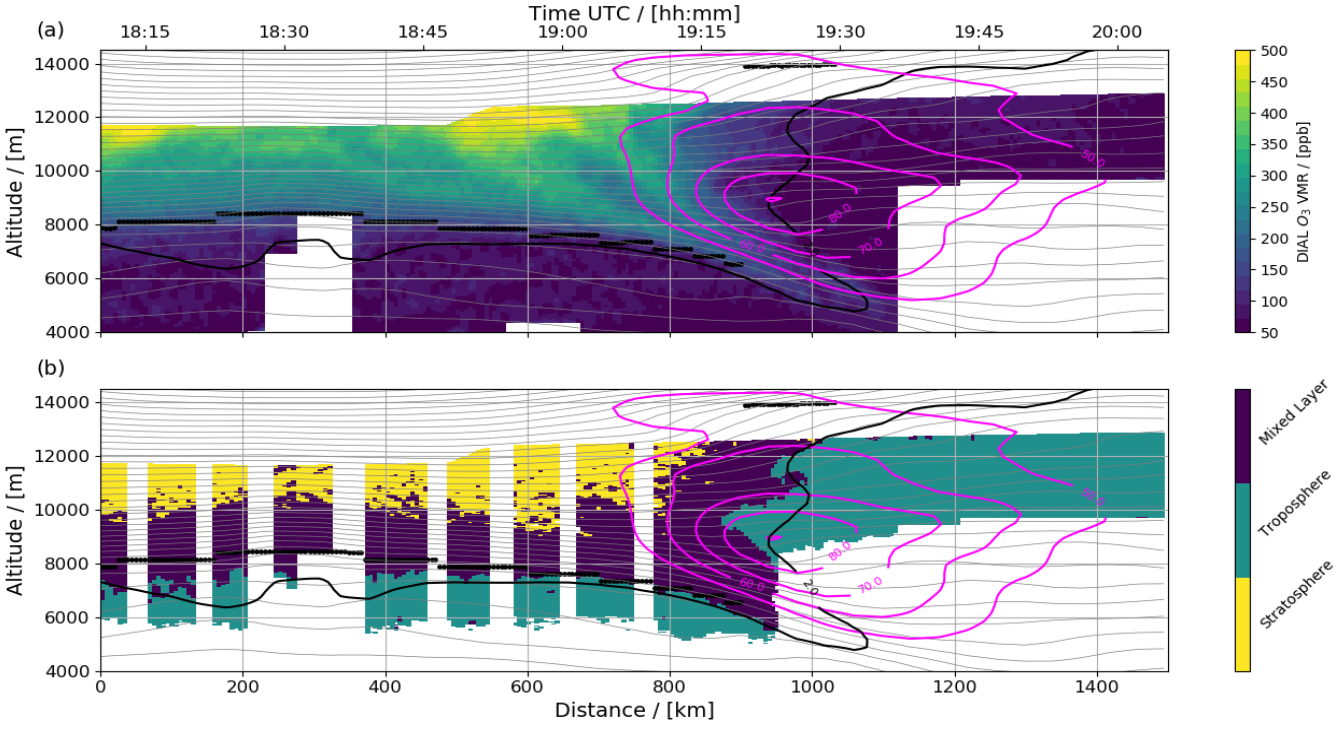

Figure 10: Vertical cross sections as in Fig. 4, but for (a) DIAL ozone volume mixing ratio (in ppb) and (b) air mass classes derived from water vapor and ozone measurements (for details see Sect. 3.3).

Following the approach by Schäfler et al. (2021), the co-located water vapor and ozone observations for four WISE flights are
380 illustrated in tracer-trace (T-T) phase space in Fig. 11. Note that the ozone and water vapor observations are given as volume mixing ratios (VMR) in the following. Three typical regions of observations can be identified. The first accumulation of tropospheric observations is characterized by low ozone VMR (typically smaller than 100 ppb) and a large spread of water vapor VMR. The second region with high ozone VMR and low water vapor VMR (< 10 ppm or < 6.2×10^{-3} g kg^{-1}) can be assigned to lower stratospheric air. Additionally, a third region in between, with intermediate chemical characteristics
385 (H_2O VMR > 10 ppm and O_3 VMR > 100 ppb) can be attributed to air masses that experienced mixing between the troposphere and stratosphere. These three classes (referred to as tropospheric, mixed and stratospheric air) are identified by defining thresholds in the T-T space. Although Schäfler et al. (2021) suggested a careful selection for individual flights, here constant

https://doi.org/10.5194/acp-2022-505
Preprint. Discussion started: 22 July 2022

Atmospheric Chemistry and Physics Discussions

threshold values (see caption of Fig. 11) are used for all four WISE flights, which is sufficiently accurate for our objective. Sensitivity tests have shown only a small dependence of the mean distribution of the classes in geometrical space. Such a re-
390 projection of the air mass classification from T-T space to geometrical space with a coherent distribution of the three classes is shown in Fig. 10b. Data below the tTP is predominantly assigned to the tropospheric air mass, while the uppermost data to the north of the jet is classified as stratospheric air. South of the jet, the flight altitude falls below the tTP and in turn only tropospheric air is detected. In between the tropospheric and the stratospheric air, the mixed air mass is following the tropopause in a layer of 2-3 km vertical extent, that appears to be vertically deeper in the tropopause fold.

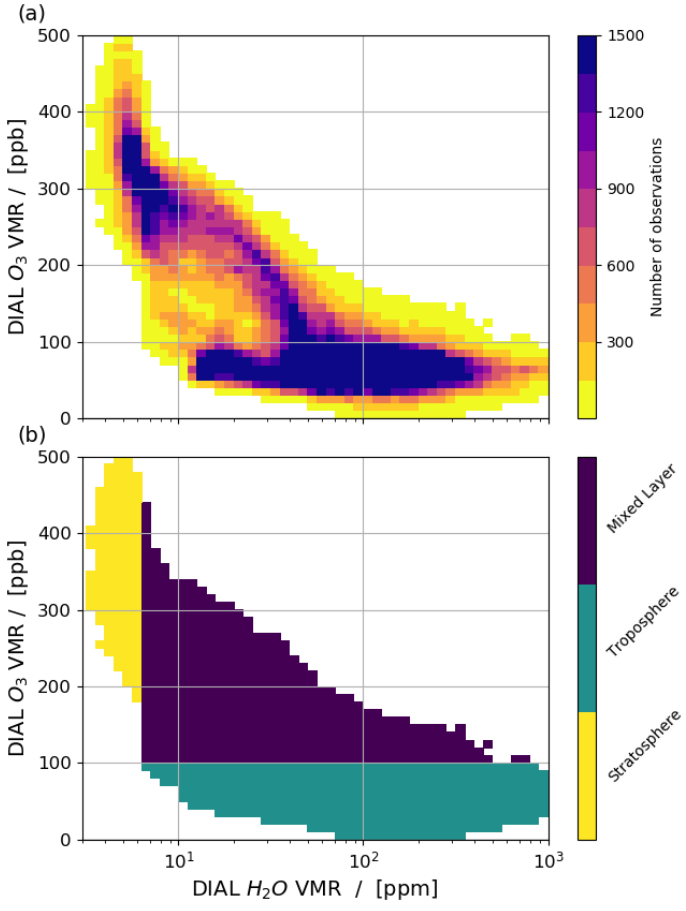

395

Figure 11: Binned distribution of water vapor and ozone observations in T-T space for four WISE flights coloured by bin-average (a) number of DIAL observations and (b) type of classified air mass with troposphere (VMR O_3 < 100 ppb and VMR H_2O > 6.5 ppm), mixed air (VMR O_3 > 100 ppb and VMR H_2O > 6.5 ppm) and stratosphere (> 100 ppb VMR O_3 and < 6.5 ppm VMR H_2O). Bin sizes are 10 ppb for VMR O_3 and 0.05 ppm for $\log_{10}$(VMR H_2O).

400

For each bin in T-T space the average humidity bias and the mean tropopause relative altitude are displayed in Fig. 12. The humidity bias is weak for both tropospheric and stratospheric air (Fig. 12a and Fig. 11b) ranging mostly between -0.25 and

https://doi.org/10.5194/acp-2022-505
Preprint. Discussion started: 22 July 2022

Atmospheric Chemistry and Physics Discussions

+0.25. In the mixed air class, the humidity bias is most pronounced (> 0.25), particularly where the water vapor mixing ratio is below 40 ppm. In the tropospheric and stratospheric air, a stronger positive/negative bias is indicated for lower/higher H_2O mixing ratios which is associated with the sharper humidity distribution in ERA5 (see discussion in Sect. 3.2.1). Figure 12b displays the tropopause relative height, which is the vertical distance to the tTP, for each bin. Across the mixed air class an increase of the tropopause relative altitude is visible corresponding to a decrease of water vapor VMR and to a increase of ozone VMR. At low water vapor (about < 10 ppm) and low ozone VMR (100-200 ppb) the transition of tropopause relative altitudes is more abrupt which is related to tTP variability across the jet stream, e.g., as visible in the uppermost part of Fig. 10b. When comparing the tropopause relative height with the distribution of the bias (Fig. 12a) it is noticeable that the average bias is particularly increased between +1 and +3 km where it ranges from 0.5 (40 %) up to 1.25 (137 %). In contrast, the mean bias is weak beyond +3 km above the tTP and below the tropopause.

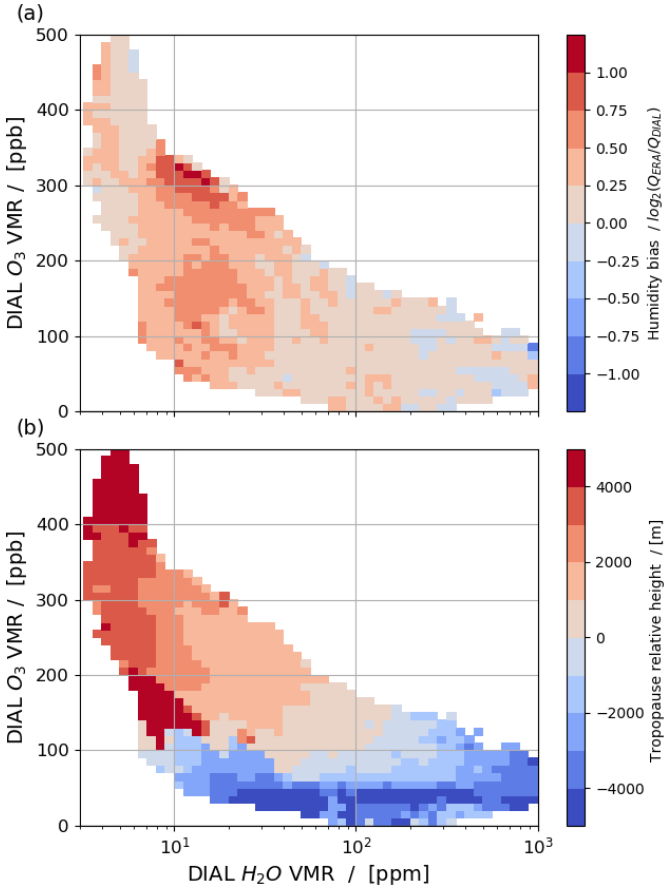

Figure 12: Binned distribution of water vapor and ozone observations in T-T space as in Fig. 11 but coloured by bin-average (a) humidity bias and (b) tropopause relative altitude.

For the considered flights the average vertical profile of the humidity bias (Fig. 13a) shows a similar structure to that of the full data set (see Fig. 5b), including the weak positive bias (0.25) in the UT with a local minimum at the tTP (+0.1; 7 %) a

https://doi.org/10.5194/acp-2022-505
Preprint. Discussion started: 22 July 2022

Atmospheric Chemistry and Physics Discussions

pronounced maximum of 0.62 (54 %) peaking at about +1 km above the tTP, and a decrease beyond. Figure 13b shows the relative proportion of the individual air masses at a given tropopause relative altitude and thus gives information about the connection between the vertical structure of the bias and the air mass classes. In the entire UT, the tropospheric air class provides the largest contribution of more than 80 % up to 500 m below the tTP. Across the tTP, the proportion of tropospheric air rapidly decreases with altitude in accordance with a rapid growth of the fraction of mixed air. This is accompanied by an increase of the bias with the altitude of the largest bias coinciding with the maximum relative contribution of the mixed air class (>90 %). Above, the relative fraction of stratospheric air grows, while the bias reduces and reaches constant values (0.2) at ~4 km above the tTP with a 65-85 % share of stratospheric air. Please note that contributions of mixed air below the tropopause and at highest altitudes may be related to falsely detected tropopause altitudes (see discussion in Sect. 4) or situations of complex tropopause structure (e.g. as shown in the second part of Fig. 10b).

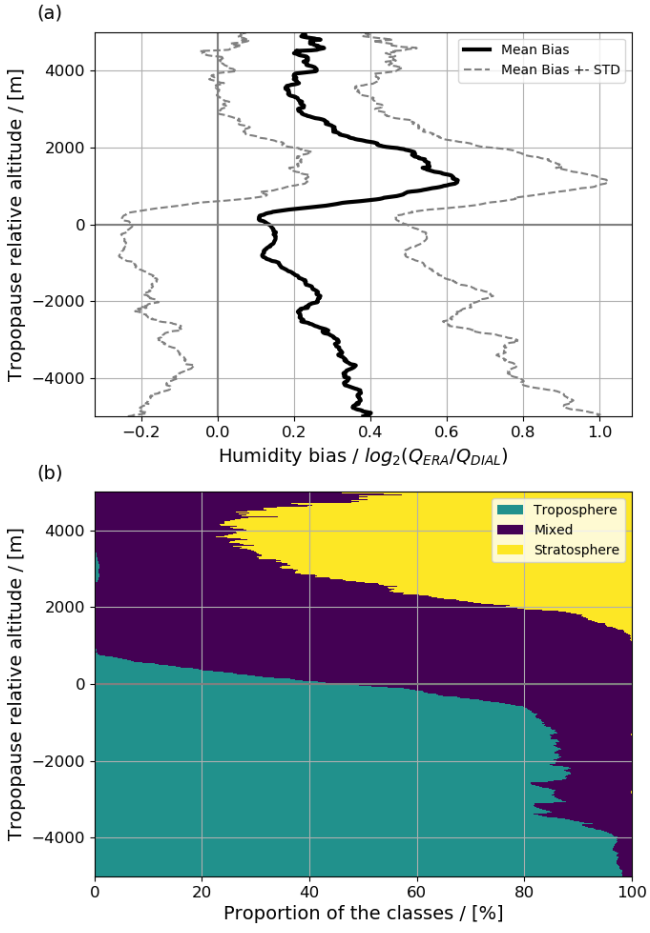

Figure 13: (a) Tropopause-relative vertical profile of the mean (thick black line) and standard deviation (thin grey dotted lines) of the humidity bias and (b) relative proportion of the individual air mass classes for four WISE flights.

https://doi.org/10.5194/acp-2022-505
Preprint. Discussion started: 22 July 2022


Atmospheric Chemistry and Physics Discussions

4 Discussion

Recent studies document a lower-stratospheric moist bias in different NWP models (e.g., Kunz et al., 2014; Dyroff et al., 2015; Kaufmann et al., 2018; Woiwode et al., 2020; Bland et al., 2021). We find a comparable bias in ERA5 reanalyses based on a comprehensive multi-campaign water vapor lidar data set comprising 41 research flights (6 campaigns) and more than 31000 vertical profiles obtained in the northern hemispheric midlatitudes during different seasons. The observations from the surface up to the LS cover four orders of magnitude and represent typical mid-latitude data for the individual seasons (e.g., Pan et al., 2000; Randel and Wu, 2010, Zahn et al., 2014; Kunz et al., 2014; Dyroff et al., 2015; Bland et al., 2021). The high data availability around the tropopause makes the data set suitable for an evaluation of NWP fields in the UTLS. Although the number of observations reduces considerably towards the highest altitudes, the data set provides a valuable extension to previous humidity data sets which exhibit increased measurement uncertainties at highest altitudes (e.g., Bland et al., 2021).

In the troposphere we find strong positive and negative biases of small spatial extent, which are likely related to insufficiently represented tropospheric transport processes, to model errors of tropospheric processes (e.g. clouds) or to the linear interpolation scheme that may have caused increased differences especially in situations of strong horizontal or vertical moisture gradients. The small positive and vertically almost constant mean bias in the UT, that ranges between +0.2 (+15 %) and +0.26 (+20 %), confirms earlier findings (Dyroff et al., 2015; Bland et al., 2021). It has to be noted that the UT bias is limited to cloud-free scenes, as DIAL humidity profile observations cannot be retrieved inside or below optical thick clouds. In agreement with Bland et al. (2021) a local minimum of the bias (< 0.2, < +15 %) is found at the tTP. Above the tropopause, our findings confirm a coherent layer of overestimated humidity in ERA5 reanalyses. The magnitude of the maximum bias of +0.63 (55 %) and its altitude of +1.3 km above the tTP is comparable to previous findings for earlier model cycles of the IFS (Dyroff et al., 2015; Kaufmann et al., 2018; Woiwode et al., 2020; Bland et al., 2021), earlier reanalysis versions (Oikonomou and O'Neill, 2006; Kunz et al., 2014) and other evaluated models (Davis et al., 2017; Bland et al., 2021). Above the maximum bias, in a region where recent studies present diverging results (Dyroff et al., 2015; Woiwode et al., 2020; Bland et al., 2021) our results corroborate a steadily decreasing bias that reduces to nearly constant and small positive values comparable to the UT. The independence of measurement error from altitude and humidity concentration allows a reliable and robust depiction of the bias at the highest altitudes.

In line with findings of Bland et al. (2021) who indicated little sensitivity of the bias to various atmospheric conditions but revealed a different depth bias for trough and ridge situations, low tTP situations (which are typically associated with troughs) exhibit a maximum bias at higher altitudes and a deeper layer of the increased bias compared to high tTP situations. The magnitude of the bias is found to be independent of the tropopause altitude. In addition, we detect a pronounced LS bias in the summer (>1.20; >130 %) which exceeds the diagnosed autumn bias by a factor of 2-3. So far, such a seasonality was only suggested in the Dyroff et al. (2015). Additional DIAL observations in spring, summer and winter would be valuable for a more comprehensive study of the seasonality of the vertical bias structure.

https://doi.org/10.5194/acp-2022-505
Preprint. Discussion started: 22 July 2022

Atmospheric Chemistry and Physics Discussions

For four flights during the WISE campaign an air mass classification using co-located H_2O and O_3 profile data (Schäfler et al., 2021) was applied to separate tropospheric (low O_3 VMR and large H_2O VMR), stratospheric (large O_3 VMR and low H_2O VMR) and mixed air (intermediate O_3 VMR and H_2O VMR). In tropopause relative coordinates, the vertical structure of the bias for the selected cases turned out to be comparable to the multi-campaign LS bias, so that these flights are considered to be representative for autumn data. We find that the bias is increased in the mixed air class representing the ExTL and that the maximum is reached at the altitude where the proportion of mixed air is highest (near 100 %). The decrease of the bias above and below is accompanied by a growth of the proportion of stratospheric and tropospheric air. The high correlation in the distribution of the bias and the ExTL gives a strong hint at the importance of the injection of moisture, either due to numerical diffusion across the tropopause or due to insufficiently modelled transport and mixing processes. As the bias in the ExTL is increased in each of the evaluated WISE flights we consider systematic uncertainties in the representation of mixing processes to play a key role for the LS bias. This supported by the finding of a deeper bias layer above troughs which are characterized by a thicker ExTL above (e.g., Hoor et al., 2002; Pan et al., 2007). In addition, the maximum bias occurs in summer when cross-tropopause mixing is strongest (Hoor et al., 2002), and finally, the bias is reduced in stratospheric background humidity at highest altitudes which are not influenced by mixing processes at the extratropical tropopause. Schäfler et al. (2022, in prep.) investigate the Lagrangian history of the observed air for the presented WISE case study on 1 October 2017 and find that the ExTL air experienced strong turbulent mixing in the jet stream during 48 h before the observation. They also find that the mixed air (in which we identified the increased bias) shows highly variable origins and transport pathways related to tropospheric weather systems which may be indicative for the relevance of different mixing processes transporting too much air into the LS. Additional co-located observations of ozone and water vapor in different seasons, near active mixing process (e.g., convection) or in the southern hemisphere where exchange at the polar jet is reduced (e.g., Bowman, 1995) could provide valuable information about the relevance of individual mixing processes and their role to form the moist bias. The presented results suggest that improving the representation of mixing at the tropopause may reduce the humidity bias and be beneficial to improve the modelling of climate and weather. Davis et al. (2017) demonstrates that various reanalyses significantly overestimate LS humidity in the extratropics. The systematic moist bias in ERA5 reanalyses has to be kept in mind for climatological studies using ERA5 humidity fields in the LS.

5 Conclusion

In this study we applied a comprehensive data set of airborne water vapor lidar profiles to investigate the representation of specific humidity in the ERA5 reanalysis across the extratropical UTLS. The main conclusions of this work are summarized below following the three research questions that were raised in the introduction:

1. *Does the multi-campaign DIAL data set add more information for a robust quantification of the LS moisture bias?*

https://doi.org/10.5194/acp-2022-505
Preprint. Discussion started: 22 July 2022


Atmospheric Chemistry and Physics Discussions

In conclusion, the presented DIAL data set with its a large number of high-accuracy and high-resolution humidity profiles measured over the North Atlantic and Europe during six research campaigns between 2013-2021 provides a valuable extension to the available observational data sets that were used to determine the lower-stratospheric bias. Beside the broad range of observed humidity values (10^{-3} to 10^{1} g kg^{-1}), especially the high data availability in the ±5 km around the tropopause makes the data suitable for the characterization of water vapor in the entire mid-latitude UTLS. The flights that were performed in different times of the year can reproduce seasonal differences in the observed humidity distributions. As the flights also cover diverse synoptic situations we consider the data to be representative for the midlatitudes. The data holds the advantage of not being assimilated by NWP and thus allows humidity errors in the ERA5 reanalysis to be evaluated independently.

2. *What is of the vertical structure of the LS moist bias in ERA5, particularly at high altitudes?*

Our analysis demonstrates that a systematic lower-stratospheric moist bias is also contained in ECMWF's most recent global reanalysis ERA5. We find that the vertical structure of the bias, that is analysed in tropopause relative coordinates, is characterized by a weak positive bias in the upper troposphere (15-20 %) and a strong overestimation of humidity that reaches a maximum (55 %) at 1.3 km above the thermal tropopause. Above this maximum we detect a steady vertical decrease of the bias towards a constant small value (15 %) beyond 4 km above the tropopause. The moist bias occurs in coherent and extended regions along the individual lidar cross-sections. The above described unique measurement characteristics of the DIAL data set together with the persistence of the bias structure in different flights and campaigns allow the vertical decline at the highest altitudes to be robustly confirmed. A high similarity for two campaigns conducted in the same region over the North Atlantic in successive years illustrates the persistence of the vertical bias structure. We find a seasonality of the bias with a maximum in summer and a minimum in winter. Lower tropopause altitudes which are typically related to troughs exhibit a deeper layer of increased bias while the bias over ridges is confined to a shallow layer.

3. *Is the moist bias correlated to the distribution of mixed air masses in the UTLS?*

For four flights of the DIAL data set co-located H_2O and O_3 profile are available and used to classify UTLS air masses according to their chemical characteristics into tropospheric, stratospheric and mixed air. We find the strongest bias at altitudes dominated by the mixed air class representing the ExTL while tropospheric or stratospheric air exhibit a smaller bias. From this correlation we deduce that insufficiently represented mixing processes and the role of numerical diffusion in ERA5 shape the vertical structure of the lower-stratospheric bias with the maximum occurring at altitudes that are most frequently affected by exchange processes between the troposphere and the stratosphere. The vertical structure of bias of the entire data set is comparable to the four flights with co-located ozone and water vapor observations. In addition, the deeper bias over troughs which typically feature a deeper ExTL, the maximum bias in summer when cross-tropopause mixing is strongest, and the reduced bias at altitudes of constant stratospheric background humidity leads to the conclusion that the findings are applicable to the mid-latitude in general. In future, it would be interesting to identify the individual mixing processes that affect the bias most and the time scales on which it is formed.

https://doi.org/10.5194/acp-2022-505
Preprint. Discussion started: 22 July 2022

Atmospheric Chemistry and Physics Discussions

Data availability

The lidar data used in this study are available through the HALO database (https://halo-db.pa.op.dlr.de/). We are grateful to ECMWF for granting access to the full-resolution ERA5 data.

Author contributions.

KK performed the data analysis, produced the figures and wrote the manuscript. AS, MWi, MWe and GC supported the interpretation of the data, contributed with ideas and commented on the paper. MWi performed the DIAL data processing.

Competing interests

The authors declare that they have no conflicts of interest.

Acknowledgements

The authors thank the individual research teams that successfully conducted the field campaigns NARVAL, NARVAL2, NAWDEX, WISE, EUREC^{4}A and Cirrus-HL which enabled us to perform this study. This work was supported by the Transregional Collaborative Research Center SFB/TRR165 “Waves to Weather" (https://www.wavestoweather.de) funded by the German Research Foundation (DFG). We further acknowledge the DFG for supporting the HALO missions within the priority program SPP 1294 "Atmospheric and Earth System Research with HALO” (https://www.halo-spp.de/). We are grateful to DLR who supported this work in the framework of the DLR project “Klimarelevanz von atmosphärischen Spurengasen, Aerosolen und Wolken” (KliSAW). We thank Andreas Dörnbrack for his valuable comments on the manuscript.

References

Bhawar, R., Di Girolamo, P., Summa, D., Flamant, C., Althausen, D., Behrendt, A., Kiemle, C., Bosser, P., Cacciani, M., Champollion, C., Di Iorio, T., Engelmann, R., Herold, C., Müller, D., Pal, S., Wirth, M., and Wulfmeyer, V.: The water vapour intercomparison effort in the framework of the Convective and Orographically-induced Precipitation Study: airborne-to-ground-based and airborne-to-airborne lidar systems. Q. J. R. Meteorol. Soc. 137, 325–348, https://doi.org/10.1002/qj.697, 2011.

Birner, T., Dörnbrack, A., and Schumann, U.: How sharp is the tropopause at midlatitudes?, Geophys. Res. Lett., 29, https://doi.org/10.1029/2002GL015142, 2002.

Bland, J., Gray, S., Methven, J., and Forbes, R.: Characterizing extratropical near-tropopause analysis humidity biases and their radiative effects on temperature forecasts, Q. J. R. Meteorol. Soc., 140, 3878-3898, https://doi.org/10.1002/qj.4150, 2021.

Brewer, A. W.: Evidence for a world circulation provided by the measurements of helium and water vapor distribution in the stratosphere, Q. J. R. Meteorol. Soc., 75, 351–363, https://doi.org/10.1002/qj.49707532603, 1949.

Bowman, K. P.: Rossby wave phase speeds and mixing barriers in the stratosphere. Part I: Observations, J. Atmos. Sci., 53, 905-918, https://doi.org/10.1175/1520-0469(1996)053<0905:RWPSAM>2.0.CO;2 1995

Chagnon, J. M., Gray, S. L., and Methven, J.: Diabatic processes modifying potential vorticity in a North Atlantic cyclone, Q. J. R. Meteorol. Soc, 139, 1270-1282, https://doi.org/10.1002/qj.2037, 2013.

Davis, S. M., Hegglin, M. I., Fujiwara, M., Dragani, R., Harada, Y., Kobayashi, C., Long, C., Manney, G. L., Nash, E. R., Potter, G. L., Tegtmeier, S., Wang, T., Wargan, K., and Wright, J. S.: Assessment of upper tropospheric and stratospheric water vapor and ozone in reanalyses as part of S-RIP, Atmos. Chem. Phys., 17, 12743–12778, https://doi.org/10.5194/acp-1712743-2017, 2017.

Dee, D. P., Uppala, S. M., Simmons, A. J., Berrisford, P., Poli, P., Kobayashi, S., Andrea, U., Balmaseda, M. A., Balsamo, G., Bauer, P., Bechtold, P., Beljaars, A. C. M., von de Berg, L., Bidlot, J., Bormann, N., Delsol, C., Dragani, R., Fuentes, M., Geer, A. J., Haimberger, L., Healy, S. B., Hersbach, H., Hólm, E. V., Isaksen, L., Kallberg, P., Köhler, M., Matricardi, M., McNally, A. P., Monge-Sanz, B. M., Morcrette, J.-J., Park, B.-K., Peubey, C., de Rosnay, P., Tavolato, C., Thépaut, J.-N., and Vitart, F.: The ERA-Interim reanalysis: configuration and performance of the data assimilation system, Q. J. R. Meteorol. Soc., 137, 553–597, https://doi:10.1002/qj.828, 2011.

Dessler, A. E., and Sherwood, S. C.: Effect of convection on the summertime extratropical lower stratosphere, J. Geophys. Res., 109, D23301, https://doi.org/10.1029/2004JD005209, 2004.

Diamantakis, M. and Flemming, J.: Global mass fixer algorithms for conservative tracer transport in the ECMWF model, Geosci. Model Dev., 7, 965–979, https://doi.org/10.5194/gmd-7-965-2014, 2014.

Dobson, G. M. B., A. W. Brewer, and B. Cwilong, The meteorology of the stratosphere, Proc. R. Soc. London Ser. A, 185, 144–175, https://doi.org/10.1098/rspa.1946.0010, 1946.

Dyroff, C., Zahn, A., Christner, E., Forbes, R., Tompkins, A. M., and van Velthoven, P. F. J.: Comparison of ECMWF analysis and forecast humidity data with CARIBIC upper troposphere and lower stratosphere observations, Q. J. Roy. Meteor. Soc., 141, 833–844, https://doi.org/10.1002/qj.2400, 2015.

ECMWF IFS Documentation – Cy41r1: Part III: Dynamics and Numerical Procedures, IFS Documentation, ECMWF, available online at: https://www.ecmwf.int/sites/default/files/elibrary/2015/9210-part-iii-dynamics-and-numerical-procedures.pdf, 2015.

Ehret, G., Hoinka, K. P., Stein, J., Fix, A., Kiemle, C., and Poberaj, G.: Low stratospheric water vapour measured by an airborne DIAL, J. Geophys. Res.-Atmos., 104, 31351–31359, https://doi.org/10.1029/1999JD900959, 1999.

Esselborn, M., Wirth, M., Fix, A., Tesche, M., and Ehret, G.: Airborne high spectral resolution lidar for measuring aerosol extinction and backscatter coefficients, Appl. Opt., 47, 346–358, https://doi.org/10.1364/AO.47.000346, 2008.

Fix, A., Steinebach, F., Wirth, M., Schäfler, A., and Ehret, G.: Development and application of an airborne differential absorption lidar for the simultaneous measurement of ozone and water vapor profiles in the tropopause region, Appl. Optics, 58, 5892–5900, https://doi.org/10.1364/AO.58.005892, 2019.

Flentje, H., Dörnbrack, A., Fix, A., Ehret, G., and Hólm, E.: Evaluation of ECMWF water vapour fields by airborne differential absorption lidar measurements: a case study between Brazil and Europe, Atmos. Chem. Phys., 7, 5033–5042, https://doi.org/10.5194/acp-7-5033-2007, 2007.

590 Forster, P. M. F., and Shine K. P.: Assessing the climate impact of trends in stratospheric water vapor, J. Geophys. Res., 29, 10-1-10-4, https://doi.org/10.1029/2001GL013909, 2002.

Fueglistaler, S., Dessler, A. E., Dunkerton, T. J., Folkins, I., Fu, Q. and Mote, P. W.: Tropical tropopause layer, Rev. Geophys., 47, RG1004, https://doi.org/10.1029/2008RG000267, 2009a.

Gettelman, A., Hoor, P., Pan, L. L., Randel, W. J., Hegglin, M. I., and Birner, T.: The extratropical upper troposphere and
595 lower stratosphere, Rev. Geophys., 49, RG3003, https://doi.org/10.1029/2011RG000355, 2011.

Gray, S., Dunning, C., Methven, J., Masato, G., and Chagnon, J.: Systematic model forecast error in Rossby wave structure, Geophys. Res. Lett., 41, 2979–2987, https://doi.org/10.1002/2014GL059282, 2014.

Grams, C. M., Wernli, H., Böttcher, M., Campa, J., Corsmeier, U., Jones, S. C., Keller, J. H., Lenz, C.-J., and Wiegand, L.: The key role of diabatic processes in modifying the upper-tropospheric wave guide: a North Atlantic case-study, Q. J. R.
600 Meteorol. Soc., 137, 2174-2193, https://doi.org/10.1002/qj.891, 2011.

Groß, S., Esselborn, M., Weinzierl, B., Wirth, M., Fix, A., and Petzold, A.: Aerosol classification by airborne high spectral resolution lidar observations, Atmos. Chem. Phys., 13, 2487–2505, https://doi.org/10.5194/acp-13-2487-2013, 2013.

Haynes, P. and Shuckburgh, E.: Effective diffusivity as a diagnostic of atmospheric transport 2. Troposphere and lower stratosphere, J. Geophys. Res., 105, 22795–22810, https://doi.org/10.1029/2000JD900092, 2000.

605 Held, I. M. and Soden, B. J.: Water vapor feedback and global warming. Annu. Rev. Energy Environ., 25, 441-475, https://doi.org/10.1146/annurev.energy.25.1.441, 2000.

Hegglin, M. I., Boone, C. D., Manney, G. L., and Walker, K. A.: A global view of the extratropical tropopause transition layer from Atmospheric Chemistry Experiment Fourier Transform Spectrometer O_3, H_2O, and CO, J. Geophys. Res.-Atmos., 114, D00B11, https://doi.org/10.1029/2008JD009984, 2009.

610 Hersbach, H., Bell, B., Berrisford, P., Hirahara, S., Horányi, A., Muñoz-Sabater, J., Nicolas, J., Peubey, C., Radu, R., Schepers, D., Simmons, A., Soci, C., Abdalla, S., Abellan, X., Balsamo, G., Bechtold, P., Biavati, G., Bidlot, J., Bonavita, M., De Chiara, G., Dahlgren, P., Dee, D., Diamantakis, M., Dragani, R., Flemming, J., Forbes, R., Fuentes, M., Geer, A., Haimberger, L., Healy, S., Hogan, R. J., Hólm, E., Janisková, M., Keeley, S., Laloyaux, P., Lopez, P., Lupu, C., Radnoti, G., de Rosnay, P., Rozum, I., Vamborg, F., Villaume, S., and Thépaut, J.-N.: The ERA5 global reanalysis, Q. J. Roy.
615 Meteor. Soc., 146, 1999-2049, https://doi.org/10.1002/qj.3803, 2020.

Hintsa, E. J., Weinstock, E. M., Dessler, A. E., Anderson, J. G., Loewenstein, M., Podolske, J. R.: SPADE H_2O measurements and the seasonal cycle of stratospheric water vapor, Geophys. Res. Lett., 21, 2559-2562, https://doi.org/10.1029/94GL01279, 1994.

Holton, J. R., Haynes, P. H., McIntyre, M. E., Douglass, A. R., Rood, R. B., and Pfister L.: Stratosphere-troposphere exchange,
620 Rev. Geophys., 33, 403–439, https://doi.org/10.1029/95RG02097, 1995.

Homeyer, C. R., Pan, L. L., and Barth, M. C.: Transport from convective overshooting of the extratropical tropopause and the role of large-scale lower stratosphere stability, J. Geophys. Res.-Atmos., 119, 2220–2240, https://doi.org/10.1002/2013JD020931, 2014.

Hoor, P., Fischer, H., Lange, L., Lelieveld, J., and Brunner, D.: Seasonal variations of a mixing layer in the lowermost stratosphere as identified by the CO-O_3 correlation from in situ measurements, J. Geophys. Res.-Atmos., 107, 4044, https://doi.org/10.1029/2000JD000289, 2002.

Hoor, P., Wernli, H., Hegglin, M. I., and Bönisch, H.: Transport timescales and tracer properties in the extratropical UTLS, Atmos. Chem. Phys., 10, 7929–7944, https://doi.org/10.5194/acp-10-7929-2010, 2010.

Jiang, J. H., Su, H., Zhai, C. X., Wu, L. T., Minschwaner, K., Molod, A. M., and Tompkins, A. M.: An assessment of upper troposphere and lower stratosphere water vapor in MERRA, MERRA2, and ECMWF reanalyses using Aura MLS observations, J. Geophys. Res.-Atmos., 120, 11468–11485, https://doi.org/10.1002/2015JD023752, 2015.

Kaufmann, S., Voigt, C., Heller, R., Jurkat-Witschas, T., Krämer, M., Rolf, C., Zöger, M., Giez, A., Buchholz, B., Ebert, V., Thornberry, T., and Schumann, U.: Intercomparison of midlatitude tropospheric and lower-stratospheric water vapor measurements and comparison to ECMWF humidity data, Atmos. Chem. Phys., 18, 16729–16745, https://doi.org/10.5194/acp-18-16729-2018, 2018.

Kiemle, C., Wirth, M., Fix, A., Ehret, G., Schumann, U., Gardiner, T., Schiller, C., Sitnikov, N., and Stiller, G.: First airborne water vapor lidar measurements in the tropical upper troposphere and mid-latitudes lower stratosphere: accuracy evaluation and intercomparisons with other instruments, Atmos. Chem. Phys., 8, 5245–5261, https://doi.org/10.5194/acp-8-5245-2008, 2008.

Kiemle C., Schäfler A., Voigt C.: Detection and Analysis of Water Vapor Transport. In: Atmospheric Physics: Background – Methods – Trends. edited by: Schumann, U., Springer-Verlag, Berlin, 169-184, https://doi.org/10.1007/978-3-642-30183-4_11, 2012.

Klepp, C., Ament, F., Bakan, S., Hirsch, L., & Stevens, B., The Next-generation Aircraft Remote sensing for VALidation studies (NARVAL) Campaign flight reports using the research aircraft HALO (The NARVAL Campaign Report). Berichte zur Erdsystemforschung / Max-Planck-Institut für Meteorologie, 164, publicly available at: https://pure.mpg.de/rest/items/item_2129055/component/file_2129139/content, last access: 30 June 2022, 2014.

Krautstrunk, M. and Giez, A.: The transition from FALCON to HALO era airborne atmospheric research, in: Atmospheric Physics: Background – Methods – Trends, edited by: Schumann, U., Springer-Verlag, Berlin, 609–624, https://doi.org/10.1007/978-3-642-30183-4_37, 2012.

Kunkel, D., Hoor, P., Kaluza, T., Ungermann, J., Kluschat, B., Giez, A., Lachnitt, H.-C., Kaufmann, M., and Riese, M.: Evidence of small-scale quasi-isentropic mixing in ridges of extratropical baroclinic waves, Atmos. Chem. Phys., 19, 12607–12630, https://doi.org/10.5194/acp-19-12607-2019, 2019.

Kunz, A., Spelten, N., Konopka, P., Müller, R., Forbes, R. M., and Wernli, H.: Comparison of Fast In situ Stratospheric Hygrometer (FISH) measurements of water vapor in the upper troposphere and lower stratosphere (UTLS) with ECMWF (re)analysis data, Atmos. Chem. Phys., 14, 10803–10822, https://doi.org/10.5194/acp-14-10803-2014, 2014.

Martius, O., Schwierz, C., and Davies, H. C.: Tropopause-Level Waveguides, J. Atmos. Sci., 67, 866–879, https://doi.org/10.1175/2009JAS2995.1, 2010.

https://doi.org/10.5194/acp-2022-505
Preprint. Discussion started: 22 July 2022


Atmospheric Chemistry and Physics Discussions

Oikonomou, E. K., and O'Neill, A.: Evaluation of ozone and water vapor fields from the ECMWF reanalysis ERA-40 during 1991–1999 in comparison with UARS satellite and MOZAIC aircraft observations, J. Geophys. Res., 111, D14109, https://doi.org/10.1029/2004JD005341, 2006.

Pan, L., Hintsa, E., Stone, E., Weinstock, E., and Randel, W.: The seasonal cycle of water vapor and saturation vapor mixing ratio in the extratropical lowermost stratosphere, J. Geophys. Res., 105, 26, 519–26, 530, https://dx.doi.org/10.1029/2000JD900401, 2000.

Pan, L. L., Randel, W. J., Gary, B. L., Mahoney, M. J., and Hintsa, E. J.: Definitions and sharpness of the extratropical tropopause: A trace gas perspective, J. Geophys. Res.-Atmos., 109, D23103, https://doi.org/10.1029/2004JD004982, 2004.

Pan, L. L., Bowman, K. P., Shapiro, M., Randel, W. J., Gao, R. S., Campos, T., Davis, C., Schauffler, S., Ridley, B. A., Wei, J. C., and Barnet, C.: Chemical behavior of the tropopause observed during the Stratosphere-Troposphere Analyses of Regional Transport experiment, J. Geophys. Res.-Atmos., 112, D18110, https://doi.org/10.1029/2007JD008645, 2007.

Randel, W. J., Wu, F., and Forster, P.: The extratropical tropopause inversion layer: Global observations with GPS data, and a radiative forcing mechanism, J. Atmos. Sci., 64, 4489–4496, https://doi.org/10.1175/2007JAS2412.1, 2007.

Randel, W. J., and Wu, F.: The polar summer tropopause inversion layer, J. Atmos. Sci., 67, 2572-2581, https://doi.org/10.1175/2010JAS3430.1, 2010.

Riese, M., Ploeger, F., Rap, A., Vogel, B., Konopka, P., Dameris, M., and Forster, P.: Impact of uncertainties in atmospheric mixing on simulated UTLS composition and related radiative effects, J. Geophys. Res.-Atmos., 117, D16305, https://doi.org/10.1029/2012JD017751, 2012.

Schäfler A., Dörnbrack A., Kiemle C., Rahm S., and Wirth M.: Tropospheric water vapour transport as determined from airborne lidar measurements, J. Atmos. Ocean. Tech., 27, 2017–2030, https://doi.org/10.1175/2010JTECHA1418.1, 2010.

Schäfler, A., Craig, G., Wernli, H., Arbogast, P., Doyle, J. D., McTaggart-Cowan, R., Methven, J., Rivière, G., Ament, F., Boettcher, M., Bramberger, M., Cazenave, Q., Cotton, R., Crewell, S., Delanoë, J., Dörnbrack, A., Ehrlich, A., Ewald, F., Fix, A., Grams, C. M., Gray, S. L., Grob, H., Groß, S., Hagen, M., Harvey, B., Hirsch, L., Jacob, M., Kölling, T., Konow, H., Lemmerz, C., Lux, O., Magnusson, L., Mayer, B., Mech, M., Moore, R., Pelon, J., Quinting, J., Rahm, S., Rapp, M., Rautenhaus, M., Reitebuch, O., Reynolds, C. A., Sodemann, H., Spengler, T., Vaughan, G., Wendisch, M., Wirth, M., Witschas, B., Wolf, K., and Zinner, T.: The North Atlantic Waveguide and Downstream Impact Experiment, B. Am. Meteorol. Soc., 99, 1607–1637, https://doi.org/10.1175/BAMS-D-17-0003.1, 2018.

Schäfler, A., Harvey, B., Methven, J., Doyle, J. D., Rahm, S., Reitebuch, O., Weiler, F., and Witschas B.: Observation of jet stream winds during NAWDEX and characterization of systematic meteorological analysis error, Mon. Weather Rev., 148, 2889–2907, https://doi.org/10.1175/MWR-D-19-0229.1, 2020.

Schäfler, A., Fix, A., and Wirth, M.: Mixing at the extratropical tropopause as characterized by collocated airborne H_2O and O_3 lidar observations, Atmos. Chem. Phys., 21, 5217-5234, https://doi.org/10.5194/acp-21-5217-2021, 2021.

https://doi.org/10.5194/acp-2022-505
Preprint. Discussion started: 22 July 2022

Schäfler, A., Sprenger, M., Wernli, H., Fix, A., and Wirth, M.: Influence of short-term synoptic-scale processes on the paired H_2O-O_3 distribution in the UTLS across a North Atlantic jet stream, Atmos. Chem. Phys., in prep., 2022.

Shapiro, M. A.: Turbulent Mixing within Tropopause Folds as a Mechanism for the Exchange of Chemical Constituents between the Stratosphere and Troposphere, J. Atmos. Sci., 37, 994–1004, https://doi.org/10.1175/1520-0469(1980)037h0994:TMWTFAi2.0.CO;2, 1980.

Shapiro, M. A., Wernli, H., Bao, J., Methven, J., Zou, X., Doyle, J., Holt, T., Donall-Grell, E., and Neiman P.*:* A planetary-scale to mesoscale perspective of the life cycles of extratropical cyclones: The bridge between theory and observations. The life cycles of extratropical cyclones., edited by: Shapiro, M. A. and Gronas, S., Amer. Meteorol. Soc*:* Boston, 139–185, 1998.

Shepherd, T. G., Polichtchouk, I., Hogan, R. J., Simmons, A. J. Report on Stratosphere Task Force, ECMWF Technical Memorandum 824, https://dx.doi.org/10.21957/0vkp0t1xx, 2018.

Stenke, A., Grewe, V., and Ponater, M.: Lagrangian transport of water vapor and cloud water in the ECHAM4 GCM and its impact on the cold bias, Clim. Dynam., 31, 491–506, https://doi.org/10.1007/s00382-007-0347-5, 2008.

Stevens, B., Ament, F., Bony, S., Crewell, S., Ewald, F., Gross, S., Hansen, A., Hirsch, L., Jacob, M., Kölling, T., Konow, H., Mayer, B., Wendisch, M., Wirth, M., Wolf, K., Bakan, S., Bauer-Pfundstein, M., Brueck, M., Delanoë, J., Ehrlich, A., Farrell, D., Forde, M., Gödde, F., Grob, H., Hagen, M., Jäkel, E., Jansen, F., Klepp, C., Klingebiel, M., Mech, M., Peters, G., Rapp, M., Wing, A. A., and Zinner, T.: A High-Altitude Long-Range Aircraft Configured as a Cloud Observatory: The NARVAL Expeditions, B. Am. Meteorol. Soc., 100, 1061–1077, https://doi.org/10.1175/BAMS-D-18-0198.1, 2019.

Stevens, B., Bony, S., Farrell, D., Ament, F., Blyth, A., Fairall, C., Karstensen, J., Quinn, P. K., Speich, S., Acquistapace, C., Aemisegger, F., Albright, A. L., Bellenger, H., Bodenschatz, E., Caesar, K.-A., Chewitt-Lucas, R., de Boer, G., Delanoë, J., Denby, L., Ewald, F., Fildier, B., Forde, M., George, G., Gross, S., Hagen, M., Hausold, A., Heywood, K. J., Hirsch, L., Jacob, M., Jansen, F., Kinne, S., Klocke, D., Kölling, T., Konow, H., Lothon, M., Mohr, W., Naumann, A. K., Nuijens, L., Olivier, L., Pincus, R., Pöhlker, M., Reverdin, G., Roberts, G., Schnitt, S., Schulz, H., Siebesma, A. P., Stephan, C. C., Sullivan, P., Touzé-Peiffer, L., Vial, J., Vogel, R., Zuidema, P., Alexander, N., Alves, L., Arixi, S., Asmath, H., Bagheri, G., Baier, K., Bailey, A., Baranowski, D., Baron, A., Barrau, S., Barrett, P. A., Batier, F., Behrendt, A., Bendinger, A., Beucher, F., Bigorre, S., Blades, E., Blossey, P., Bock, O., Böing, S., Bosser, P., Bourras, D., Bouruet-Aubertot, P., Bower, K., Branellec, P., Branger, H., Brennek, M., Brewer, A., Brilouet, P.-E., Brügmann, B., Buehler, S. A., Burke, E., Burton, R., Calmer, R., Canonici, J.-C., Carton, X., Cato Jr., G., Charles, J. A., Chazette, P., Chen, Y., Chilinski, M. T., Choularton, T., Chuang, P., Clarke, S., Coe, H., Cornet, C., Coutris, P., Couvreux, F., Crewell, S., Cronin, T., Cui, Z., Cuypers, Y., Daley, A., Damerell, G. M., Dauhut, T., Deneke, H., Desbios, J.-P., Dörner, S., Donner, S., Douet, V., Drushka, K., Dütsch, M., Ehrlich, A., Emanuel, K., Emmanouilidis, A., Etienne, J.-C., Etienne-Leblanc, S., Faure, G., Feingold, G., Ferrero, L., Fix, A., Flamant, C., Flatau, P. J., Foltz, G. R., Forster, L., Furtuna, I., Gadian, A., Galewsky, J., Gallagher, M., Gallimore, P., Gaston, C., Gentemann, C., Geyskens, N., Giez, A., Gollop, J., Gouirand, I., Gourbeyre, C., de Graaf, D., de Groot, G. E., Grosz, R., Güttler, J., Gutleben, M., Hall, K., Harris, G., Helfer, K. C.,

https://doi.org/10.5194/acp-2022-505
Preprint. Discussion started: 22 July 2022

Henze, D., Herbert, C., Holanda, B., Ibanez-Landeta, A., Intrieri, J., Iyer, S., Julien, F., Kalesse, H., Kazil, J., Kellman, A., Kidane, A. T., Kirchner, U., Klingebiel, M., Körner, M., Kremper, L. A., Kretzschmar, J., Krüger, O., Kumala, W., Kurz, A., L'Hégaret, P., Labaste, M., Lachlan-Cope, T., Laing, A., Landschützer, P., Lang, T., Lange, D., Lange, I., Laplace, C., Lavik, G., Laxenaire, R., Le Bihan, C., Leandro, M., Lefevre, N., Lena, M., Lenschow, D., Li, Q., Lloyd, G., Los, S., Losi, N., Lovell, O., Luneau, C., Makuch, P., Malinowski, S., Manta, G., Marinou, E., Marsden, N., Masson, S., Maury, N., Mayer, B., Mayers-Als, M., Mazel, C., McGeary, W., McWilliams, J. C., Mech, M., Mehlmann, M., Meroni, A. N., Mieslinger, T., Minikin, A., Minnett, P., Möller, G., Morfa Avalos, Y., Muller, C., Musat, I., Napoli, A., Neuberger, A., Noisel, C., Noone, D., Nordsiek, F., Nowak, J. L., Oswald, L., Parker, D. J., Peck, C., Person, R., Philippi, M., Plueddemann, A., Pöhlker, C., Pörtge, V., Pöschl, U., Pologne, L., Posyniak, M., Prange, M., Quiñones Meléndez, E., Radtke, J., Ramage, K., Reimann, J., Renault, L., Reus, K., Reyes, A., Ribbe, J., Ringel, M., Ritschel, M., Rocha, C. B., Rochetin, N., Röttenbacher, J., Rollo, C., Royer, H., Sadoulet, P., Saffin, L., Sandiford, S., Sandu, I., Schäfer, M., Schemann, V., Schirmacher, I., Schlenczek, O., Schmidt, J., Schröder, M., Schwarzenboeck, A., Sealy, A., Senff, C. J., Serikov, I., Shohan, S., Siddle, E., Smirnov, A., Späth, F., Spooner, B., Stolla, M. K., Szkółka, W., de Szoeke, S. P., Tarot, S., Tetoni, E., Thompson, E., Thomson, J., Tomassini, L., Totems, J., Ubele, A. A., Villiger, L., von Arx, J., Wagner, T., Walther, A., Webber, B., Wendisch, M., Whitehall, S., Wiltshire, A., Wing, A. A., Wirth, M., Wiskandt, J., Wolf, K., Worbes, L., Wright, E., Wulfmeyer, V., Young, S., Zhang, C., Zhang, D., Ziemen, F., Zinner, T., and Zöger, M.: EUREC^{4}A, Earth Syst. Sci. Data, 13, 4067–4119, https://doi.org/10.5194/essd-13-4067-2021, 2021.

Stohl, A., Bonasoni, P., Cristofanelli, P., Collins, W., Feichter, J., Frank, A., Forster, C., Gerasopoulos, E., Gaggeler, H., James, P., Kentarchos, T., Kromp-Kolb, H., Kruger, B., Land, C., Meloen, J., Papayannis, A., Priller, A., Seibert, P., Sprenger, M., Roelofs, G. J., Scheell, H., E. Schnabel, C., Siegmund, P., Tobler, L., Trickl, T., Wernli, H., Wirth, V., Zanis, P., and Zerefos, C.: Stratosphere-troposphere exchange: A review, and what we have learned from STACCATO, J. Geophys. Res.-Atmos., 108, 8516, https://doi.org/10.1029/2002JD002490, 2003.

Trickl, T., Vogelmann, H., Fix, A., Schäfler, A., Wirth, M., Calpini, B., Levrat, G., Romanens, G., Apituley, A., Wilson, K. M., Begbie, R., Reichardt, J., Vömel, H., and Sprenger, M.: How stratospheric are deep stratospheric intrusions? LUAMI 2008, Atmos. Chem. Phys., 16, 8791–8815, https://doi.org/10.5194/acp-16-8791-2016, 2016.

Wirth, M., Fix, A., Mahnke, P., Schwarzer, H., Schrandt, F., and Ehret, G.: The airborne multi-wavelength water vapour differential absorption lidar WALES: system design and performance, Appl. Phys. B, 201–213, https://doi.org/10.1007/s00340-009-3365-7, 2009.

World Meteorological Organization (WMO), Meteorology – A three-dimensional science, WMO Bull., 6, 134–138, 1957.

Woiwode, W., Dörnbrack, A., Polichtchouk, I., Johansson, S., Harvey, B., Höpfner, M., Ungermann, J., and Friedl-Vallon, F.: Technical note: Lowermost-stratospheric moist bias in ECMWF IFS model diagnosed from airborne GLORIA observations during winter/spring 2016, Atmos. Chem. Phys., 20, 15379–15387, https://doi.org/10.5194/acp-20-15379-2020, 2020.

https://doi.org/10.5194/acp-2022-505
Preprint. Discussion started: 22 July 2022

Atmospheric Chemistry and Physics Discussions

Zahn, A., Christner, E., van Velthoven, P. F. J., Rauthe-Schoch, A., and Brenninkmeijer, C. A. M.: Processes controlling water
760 vapor in the upper troposphere/lowermost stratosphere: An analysis of 8 years of monthly measurements by the IAGOS-CARIBIC observatory, J. Geophys. Res.-Atmos., 119, 11505–11525, https://doi.org/10.1002/2014JD021687, 2014.